Submitted to the International Europhysics Conference on High Energy Physics HEP99,
Tampere, Finland, July 1999

Study of Differential Dijet Event Distributions and Determination of α_s in Deeply Inelastic Scattering at Large Q^2

H1 Collaboration

Abstract

Events with a dijet topology are studied in deeply inelastic scattering at HERA in the kinematic range $Q^2 > 150$ GeV^2. The distribution of jet quantities such as jet polar angles, jet resolution y_2, and other jet variables are measured in different ranges of Q^2 using the modified Durham algorithm and the factorizable k_T algorithm. The jet distributions measured with the modified Durham algorithm are compared with the predictions of QCD Monte Carlo models. Different variants of the models ARIADNE and LEPTO are unable to describe all features of the data. The best description is obtained with HERWIG. Both the modified Durham algorithm and the factorizable k_T algorithm are used to select two additional event samples with jets of mean transverse energy in the Breit frame, $\langle E_T^{Breit} \rangle$, of $\sim$10 GeV. Perturbative QCD predictions in next-to-leading order are found to describe the corresponding jet distributions well with either Q or $\langle E_T^{Breit} \rangle$ chosen as the renormalization scale. The value of the strong coupling constant α_s is determined with both jet algorithms. The running of α_s as a function of the renormalization scale is measured for the scales Q and $\langle E_T^{Breit} \rangle$.

Abstract: 157
Parallel sessions: 1
Plenary sessions: 1

Electronic Access: http://www-h1.desy.de/publications/

1 Introduction

This analysis investigates the hadronic final state in deeply inelastic scattering (DIS) at HERA. Jet event rates and related jet variables are used as the observables. The photon virtuality Q^2 of the selected DIS events was chosen to be larger than 150 GeV^2. In this regime measurements of jet distributions and determinations of the strong coupling constant α_s have been performed in previous analyses [1, 2, 3]. These illustrated the potential for the fundamental testing of the theory of strong interactions, QCD, but also highlighted the limitations of such studies. Two major difficulties are the inability of Monte Carlo (MC) models to describe the complex hadronic final state at HERA precisely, and the large renormalization scale uncertainties of perturbative QCD calculations in next-to-leading order (NLO).

These and other issues are discussed in detail in this paper. The prospects for a deeper understanding of jet structures are promising. Most importantly, the collected data sample has been increased by a factor of ~ 5. This makes it possible to measure the distributions of jet observables in several bins of Q^2 in contrast to the analyses presented in [1, 2, 3]. These analyses were exclusively based on the modified JADE algorithm [4] applied in the laboratory frame. Here two different jet algorithms, the modified Durham algorithm (applied in the laboratory frame) and the factorizable k_T algorithm [5] (applied in the Breit frame) are used. These two algorithms may be expected to behave differently in many respects which makes their comparison interesting. Improved measurements of F_2 and updated extractions of the parton density functions are available. New versions of the MC models LEPTO [6] and ARIADNE [7] have been released leading to substantial changes and improvements [8].

This analysis consists of two parts. Firstly, a systematic comparison of the measured jet distributions with the predictions of the MC models LEPTO, ARIADNE and HERWIG [9] is presented. A new jet algorithm, the modified Durham algorithm, is introduced and is used for the first time at HERA. A sample of dijet events is selected which contains $\sim 1/3$ of the DIS events. The statistical and the systematic precision of the measured jet distribution is high and the differences between the various models can easily be resolved.

Secondly, the description of jet distributions by perturbative QCD calculations in NLO is investigated. Here, two more restrictive dijet event samples with jets of mean transverse energy in the Breit frame, $\langle E_T^{Breit} \rangle$, of ~ 10 GeV are selected. The selection of events with pronounced jet structures is motivated by the wish to minimize the renormalization scale uncertainties of the NLO calculations, to reduce the size of hadronization corrections and to reduce the effect of the model uncertainties in general. In [1, 2, 3] less pronounced jet structures had to be selected owing to the smaller data volumes. The jet distributions are measured with the modified Durham algorithm (as above) and the factorizable k_T algorithm. The measured jet distributions are directly sensitive to the value of the strong coupling constant which is extracted in different regions of Q^2. Furthermore, we study the effects of two different choices of renormalization scale, Q or $\langle E_T^{Breit} \rangle$, and test the running of α_s as a function of the renormalization scale for the scales Q and $\langle E_T^{Breit} \rangle$.

In addition to α_s, the jet distributions calculated in NLO also depend on the knowledge of the proton's parton densities the determination of which is (partly) based on measurements by experiments other than H1. In order to extract the parton densities, a value of $\alpha_s(M_Z^2)$ must be assumed and it is important that this assumption does not bias our fit result of α_s. These two issues are discussed in detail together with the other major sources of uncertainties.

2 Event selection

This analysis is based on the data sample recorded in the data taking periods '95–'97 with the H1 detector at HERA. In this period HERA was operated with positron and proton beams of 27.5 and 820 GeV, respectively, corresponding to a centre–of–mass energy of $\sqrt{s} = 300$ GeV. The integrated luminosity collected was $\sim$ 35 pb^{-1}.

The components of the H1 detector [10] most relevant here are the central tracking system and the liquid argon calorimeter. Some of their features are briefly given below.

The central tracking system is used to determine the ep collision point and to aid the identification of the scattered positron. It is surrounded by a liquid argon sampling calorimeter covering a polar angle range of $4^\circ < \theta < 154^\circ$. The polar angle θ is measured with respect to the incoming proton beam which is defined to point in the $+z$ direction. The electromagnetic and hadronic sections of the liquid argon calorimeter correspond in total to a depth of 4.5 to 8 interaction lengths. The energy resolution of the liquid argon calorimeter for electrons and hadronic showers is $\sigma/E = 12\%/\sqrt{E(\mathrm{GeV})} \oplus 1\%$ and $\sigma/E = 50\%/\sqrt{E(\mathrm{GeV})} \oplus 2\%$, respectively [11]. The absolute energy scale for hadronic energy depositions is known to better than 4%, and that for electromagnetic energy depositions to better than 3%.

The selection of neutral current DIS events in this analysis is similar to that of [2]. Only the main selection criteria are briefly mentioned below. The measured z coordinate of the primary event vertex is required to be within a distance of $\pm$30 cm from the nominal ep collision point. The summed energy E and longitudinal momentum components P_z of all reconstructed clusters, each assumed to be massless, must fulfil $30 < E{-}P_z < 70$ GeV. A scattered electron with polar angle $\theta_e < 150^\circ$ must have been identified in the liquid argon calorimeter. The Q^2 range is restricted to $Q^2 > 150$ GeV^2 where Q^2 is determined from the scattered positron energy and polar angle. The inelasticity y_e, calculated from the scattered positron energy and polar angle, is required to be smaller than 0.7; y_{da}, calculated using the double angle method [12], is required to be larger than 0.1. The inelasticity is defined by $y = Q^2/sx$ where s is the centre-of-mass energy squared and x is related to the fraction of the proton momentum carried by the struck quark.

After application of these cuts we obtain a sample of $\sim 60\,000$ DIS events with a negligible number of background events.

Further cuts are applied to select three different samples of dijet events. These cuts and the definition of the jet algorithms are described in the next section.

3 Selection of the multi–jet event samples and definition of jet observables

Two different jet algorithms, the modified Durham algorithm and the factorizable k_T algorithm [5], are applied to reconstruct hadronic jets from the energy depositions in the liquid argon calorimeter. Calorimeter clusters that are not related to the hadronic final state are rejected by the following quality cuts: hadronic clusters must be separated from the positron candidate by an angle greater than 10°; clusters with an angle of larger than 50° with respect to their closest neighbouring cluster are rejected. For the modified Durham algorithm, the polar angle, θ_{clus}, of a cluster is required to satisfy $\theta_{clus} > 7°$ which improves the resolution of the reconstructed jet quantities.

Modified Durham algorithm
The modified Durham algorithm is the analogue to the modified JADE algorithm [4] which has been used in a number of analyses at HERA. It is applied in the laboratory frame. The algorithm is modified compared with the version used in e^+e^-–annihilation in two respects: the cluster that is attributed to the scattered positron is removed; a massless four–vector is determined which is treated as an additional cluster by the jet algorithm to account for the longitudinal momentum carried by the proton remnant escaping through the beam pipe.

The jet algorithm calculates the scaled quantity $k^2_{T,ij}/W^2$ of pairs of clusters or 'proto' jets i, j, where W^2 is the total invariant mass squared of all clusters entering the jet algorithm. The definition of $k^2_{T,ij}$ is taken to be $2\min(E^2_i, E^2_j)\,(1 - \cos\theta_{ij})$. Here E_i and E_j are the energies of the clusters i and j, and θ_{ij} is the angle between them. The modified JADE algorithm, in contrast, replaces $k^2_{T,ij}$ by $m^2_{ij} = 2E_iE_j\,(1 - \cos\theta_{ij})$.

The jet algorithm combines the pair of clusters i, j with the minimum $k^2_{T,ij}/W^2$ to be a 'proto' jet by adding the four–momenta p_i and p_j. In the present analysis as in [2] this prescription is repeated iteratively for the remaining clusters and 'proto' jets up to the point where exactly (2+1) jets remain. (The notation '+1' refers to the proton remnant jet.) The smallest $k^2_{T,ij}/W^2$ given by any combination of the (2+1) jets is defined to be the observable y_2. The y_2 distribution, $1/N_{DIS}\; dn/dy_2$, where N_{DIS} is the number of deep–inelastic scattering events passing the selection of section 2, is called the differential (2+1) jet event rate.

Factorizable k_T algorithm
The factorizable k_T algorithm is applied to the clusters boosted to the Breit frame. In the Breit frame the exchanged virtual photon is purely space–like and its four–momentum is $\{0, 0, 0, -Q\}$. The momentum of a particle in the Breit frame and in the hadronic centre–of–mass frame is related by a boost along the $\gamma^\star$p axis. It should be noted that the observation of jet structures with large E_T^{Breit} is indicative for hard QCD radiation while large transverse energies in the laboratory frame may trivially be needed to compensate for the E_T of the scattered electron. The factorizable k_T algorithm uses *two* distance variables $k^2_{T,\,i,j}$ and $k^2_{T,\,i}$. The definition of $k^2_{T,\,i,j}$, the relative k^2_T between the clusters or 'proto' jets i and j, is identical with that of the modified Durham algorithm; $k^2_{T,\,i}$, the k^2_T relative to the proton axis, is defined as $2E^2_i(1 - \cos\theta_i)$ where θ_i is the polar angle relative to the proton axis.

The jet algorithm determines the minimum values of $k^2_{T,\,i,j}$ and $k^2_{T,\,i}$. If $k^2_{T,\,i,j}$ is smaller than $k^2_{T,\,i}$ the pair of clusters i, j is combined by adding the four–momenta p_i and p_j. Otherwise ($k^2_{T,\,i,j} > k^2_{T,\,i}$) the particle i is considered to belong to the proton remnant and is ignored in the following. Again this prescription is repeated iteratively, in the present analysis, for the remaining clusters and 'proto' jets up to the point where exactly two jets remain. Now y_2 is defined to be the jet distance $k^2_{T,\,i,j}$ divided by a fixed scale of 100 GeV^2.

3.1 Selection of the dijet event samples

Three different event samples with jets of varying hardness are selected:

- **Sample 1** contains events with $y_2 > 0.001$ as given by the *modified Durham* algorithm. This jet sample contains $\sim 1/3$ of the selected DIS events. It is mainly used to study the description of the data by the MC models. The mean transverse jet energy in the Breit frame for this sample is $\langle E_T^{Breit} \rangle \sim 5$ GeV.

- **Sample 2** contains events with $y_2 > 0.005$ as given by the *modified Durham* algorithm. This jet sample contains $\sim 1/10$ of the selected DIS events. The mean transverse jet energy is $\langle E_T^{Breit} \rangle \sim 10$ GeV. This sample of events with pronounced jet structures is used for the comparison with perturbative QCD predictions in NLO and for the determination of α_s.

- **Sample 3** contains events with $y_2 > 0.8$ as given by the *factorizable k_T* algorithm. Again, this jet sample contains $\sim 1/10$ of the selected DIS events, and its mean transverse jet energy is also $\langle E_T^{Breit} \rangle \sim 10$ GeV. This sample is also used for the comparison with perturbative QCD predictions in NLO and for the determination of α_s.

The polar angles of the two (non–remnant) jets have to satisfy $10° < \theta_{jet} < 140°$ in the laboratory frame for all three jet samples otherwise the event is not considered.

3.2 Definition of jet observables

Five observables are studied in the analysis: y_2; the polar angles of the most forward and the most backward (non–remnant) jets in the laboratory frame, θ_{fwd} and θ_{bwd}; z_p and x_p. Distributions of these observables are measured for any of the three jet samples defined above. The variable y_2 is given by the minimum k_T^2 of any combination of the (2+1) jets divided by W^2 for the *modified Durham* algorithm. It is given by the minimum k_T^2 of the two (non–remnant) jets divided by 100 GeV^2 for the *factorizable k_T* algorithm (see above). The definitions of z_p and x_p are

$$z_p \equiv \min_{i=1,2} E_i \, (1 - \cos\theta_i) / \sum_{i=1,2} E_i \, (1 - \cos\theta_i) \quad \text{and} \quad x_p \equiv \frac{Q^2}{Q^2 + m_{12}^2} \,,$$

where E_i and θ_i are the energies and polar angles of the two (non–remnant) jets remaining after the clustering of the jet algorithm, and m_{12} is the corresponding invariant dijet mass. The jet energies and polar angles in the laboratory frame are used for both algorithms.

The same definition of the jets and of the jet variables are used for the analysis of the data and of the Monte Carlo events after detector simulation. In events simulated at the hadron or parton level and in the NLO calculations, the jet algorithm is applied to hadron or parton four–momenta, respectively. The same cuts are applied to select the corresponding dijet event samples. For the Durham algorithm, the polar angle cut of $7°$ which is applied for clusters is also applied for hadrons and partons.

4 Correction of the data

The data are corrected for the effects of detector acceptance, detector resolution, and for the effects of QED radiation.

In addition, the size of hadronization effects is determined in order to compare the NLO calculations valid for partons with the hadronic data distributions. The corresponding hadronization correction factors are applied on top of the NLO calculations in any of the following comparisons of NLO and data distributions.

4.1 Correction for detector effects

Detector effects are corrected using either of the Monte Carlo models LEPTO, version 6.5, without soft-colour-interactions (SCI, see below) and ARIADNE, version 4.08. The models are incorporated in DJANGO [13], version 6.2, which simulates radiative QED effects. The generated events were passed through a full simulation of the H1 detector. For each model an event sample was generated that was $\sim$ 3 times larger than that of the experimental data.

The procedure for the correction of detector effects is identical for the jet samples two and three and is first described for these samples. The correction of the y_2 distribution is performed with the method of regularized unfolding of [14] which is also used and briefly described in [2]. The use of an unfolding method seems appropriate for the y_2 distribution since it is steeply falling and since cuts in y_2 are applied to define the jet samples. As a consistency check a bin–by–bin correction for the y_2 distribution was investigated which led to differences of at most 12% and on average to much smaller deviations compared with the unfolding method. Integrating over the corrected y_2 distribution, $1/N_{DIS}\ dn/dy_2$, the corrected fraction of jet events may be determined. It differed by typically 2% between the two correction methods.

The other distributions, θ_{fwd} and θ_{bwd}, z_p and x_p, which are less steep and which have a better resolution are corrected with bin–by–bin correction factors. In oder to make sure that the integral of all distributions corresponds to that of the unfolded y_2 distribution, an additional global correction factor of at most 2% (see above) is applied. For the jet samples two and three which are used for the comparison with the NLO calculations and for the determination of α_s, the resolution of the polar angles is 3–4°. The resolution of z_p and x_p is $\sim 35\%$, that of y_2 is $\sim 50\%$.

The jet sample 3, for which weaker cuts are applied, has a slightly worse resolution. Here, the additional first two bins of the y_2 distribution are corrected by correction factors, as are all other distributions. The chosen bin sizes match the resolution of the given variables. A measure for the reconstruction purity of a given jet observable is the fraction of events where the value of the observable reconstructed from detector objects and that calcuated from hadrons fall in the same bin. The typical reconstruction purity estimated with LEPTO and ARIADNE is 60–80% in each bin for any variable (and for any of the jet samples).

The average of the corrected jet distributions corrected with LEPTO or ARIADNE is taken as the final corrected result.

4.2 Correction for QED radiation

The effects of QED radiation are considered by multiplying the distributions obtained above by correction factors. These factors are obtained from the ratio of the Monte Carlo distributions generated with and without inclusion of QED effects.

The same models that are used for the estimation of the detector effects are used again but much larger event samples were generated. Again the average of the correction factors from LEPTO and ARIADNE is taken for the final correction.

4.3 Hadronization corrections

The hadronization correction factors are determined for each of five different sets of Monte Carlo models: LEPTO 6.5 without soft–colour–interactions; the tuned version of LEPTO 6.5.2β discussed in section 5; ARIADNE 4.08; ARIADNE 4.10 and HERWIG 5.9. The correction factor is given by the respective jet distribution as determined from hadrons divided by that determined from the partons after the parton shower. The average correction factor of those five models is taken for the final correction. The hadronization correction for the y_2 distribution decreases with increasing Q^2. It is roughly 20, 15 and 10% in the lowest, medium and highest Q^2 range for the factorizable k_T algorithm. The average spread between the correction factors of the different models is $\sim 4\%$.

4.4 Systematic errors

There are three main sources of systematic errors that influence the measured jet distributions: the model dependence of the detector and QED corrections, and the uncertainties of the energy calibration of the liquid argon calorimeter for electrons and those for hadrons.

Correction for detector effects and QED radiation
The average of the corrected jet distributions corrected with LEPTO or ARIADNE is taken as the final result. The difference of the average to the corrected distribution from either model alone is taken as the error due to the model dependence of the detector correction and of the QED correction. This results in a typical model dependence of $\sim 6\%$ which is roughly of the same size for all three jet samples.

Hadronic energy calibration
The uncertainty of the hadronic energy scale of the liquid argon calorimeter is $\pm 4\%$. This influences the number of events in the respective jet sample due to the cut in y_2. The resulting uncertainty is typically $\sim 5\%$ for jet sample one and $\sim 10\%$ for jet samples two and three.

Electron energy calibration
The uncertainty of the electromagnetic energy scale is $\pm 3\%$ in this analysis. The precise measurement of the electron kinematics is in particular important for the factorizable k_T algorithm in order to boost from the laboratory frame into the Breit frame of reference reliably. The average error assigned due to the uncertainty in the electromagnetic energy scale is $\sim 7\%$ for the factorizable k_T algorithm. The distributions measured with the Durham algorithm, which is

applied in the laboratory frame, is less sensitive to the uncertainty in the electromagnetic energy scale. Here, the average error is $\sim 2\%$.

In conclusion, the precision of the jet distributions of the jet sample one is considerably higher than that of the jet samples two and three. This is due in part to the smaller statistical error but the uncertainty of the hadronic energy scale also turns out to have less effect. In comparison to the k_T algorithm used in jet sample three, the reduced sensitivity to the electron calibration is also helpful.

5 Comparison with QCD Monte Carlo models

In this section, the jet distributions measured with the modified Durham algorithm based on the jet sample one are presented and are compared with the predictions of various QCD Monte Carlo models. The parton densities of GRV94HO [15] were used in the comparison.

5.1 Comparison with ARIADNE

ARIADNE models the QCD cascade by emitting gluons from a chain of independently radiating colour dipoles, correcting the first emission to reproduce the first order matrix elements. The phase space for parton radiation is suppressed in comparison with the situation in e^+e^- annihilation since the proton remnant (unlike a quark in e^+e^- annihilation) is treated as an extended object. Furthermore the struck quark is treated as an extended object leading to an additional phase space restriction for gluon radiation. The hadronization in ARIADNE is performed using the Lund string model [16].

In the version 4.08 of ARIADNE, the phase space reduction due to the size of the proton leads not only to the suppression of the gluon radiation in the target hemisphere but, for large Q^2, also to the suppression in the current region of the Breit frame. The latter feature was removed in ARIADNE, version 4.10.

The measured distribution of the polar angle of the backward jet, θ_{bwd}, is shown in Figure 1 together with the model predictions of the ARIADNE versions 4.10 and 4.08. The relative precision of the data points is typically better than 5%. A significant shift of the distributions to smaller angles is observed with increasing Q^2. Both model versions fail to describe the data well.

ARIADNE 4.08 does not reproduce the Q^2 dependence of the data. The predictions of ARIADNE 4.08 are above the data distributions for $150 < Q^2 < 275$ GeV^2, they agree well with the data for $275 < Q^2 < 575$ GeV^2, and they fall below the data in the range $575 < Q^2 < 5000$ GeV^2. ARIADNE 4.10 predicts too large a number of dijet events with $y_2 > 0.001$ in any Q^2 region, such that the model distributions overshoot the data significantly.

5.2 Comparison with LEPTO

LEPTO is based on the exact first order matrix elements followed by higher order radiation approximated by leading logarithm parton showers based on the DGLAP evolution equations. The divergences of the matrix element are suppressed by a cutoff in z_q^{min} and $\hat{s}^{min}$, the invariant mass squared of the two partons generated by the matrix element. Like ARIADNE, LEPTO models the hadronization according to the Lund string model. In order to describe diffractive events, another non-perturbative mechanism, the soft-colour-interactions (SCI), was implemented in LEPTO. This turned out to have a significant effect on the description of the hadronic final state in the non-diffractive events at large Q^2 as is illustrated below.

In Figure 2 the predictions of LEPTO, version 6.5, with soft-colour-interactions are seen to be twice as high as the data distributions at low θ_{fwd}. A modification of the SCI model has been proposed in [17] and is implemented in LEPTO, version 6.5.2β. While the probability for a soft-colour-interaction is kept fixed in the original model, soft-colour interactions are now suppressed depending on the difference in area spanned by the possible string configurations (after or before a soft-colour interaction). The corresponding predictions of LEPTO, version 6.5.2β, are also shown in Figure 2. They give a much improved description of the data distributions although significant deviations from the data are still visible. A similar description of the data is observed when the probability for a soft-colour-interaction is assumed to be zero in LEPTO, version 6.5.

In order to improve the data description by LEPTO further, a systematic optimization of the model parameters z_q^{min} and $\hat{s}^{min}$ is tried. The best description of the data is achieved by setting the cutoff parameters z_q^{min} and $\hat{s}^{min}$ to 0.04 and 1.0 GeV^2 which is to be compared with the default values of 0.04 and 25.0 GeV^2 [18]. The effect is shown in Figure 3. The optimized parameter values lead to an improved description of the data (full line). It is obvious that in either case, LEPTO has considerable difficulties in describing the z_p distribution.

In Figure 3, the data are also compared with a perturbative QCD calculation in NLO obtained from DISENT [19] (see the next section). A correction factor considering hadronization effects was added to the NLO calculation. Given the loose jet hardness cuts of the jet sample one, QCD in NLO would not necessarily be expected to describe the distribution well. However it performs better than ARIADNE and LEPTO.

5.3 Comparison with HERWIG

HERWIG is based on a coherent parton shower algorithm with a detailed simulation of QCD interference and spin effects and with additional first order matrix element corrections. The hadronization is performed with the cluster fragmentation model [20]. In contrast to the default version of HERWIG, we use the LO and not the NLO formula for α_s in HERWIG.

A fair description of the measured jet distributions is obtained with HERWIG, version 5.9.

The predictions of HERWIG are compared with the measured distributions of y_2, z_p, θ_{fwd} and θ_{bwd} in the range $Q^2 > 150$ GeV^2 in Figure 4. The model predictions of ARIADNE 4.08 and LEPTO 6.5.2β with tuned parameters are also shown. In the range $Q^2 > 150$ GeV^2, these model versions give the best description of the data. The poor Q^2 dependence of the dijet events in ARIADNE 4.08 is less important here due to an approximate cancelation effect between the lowest and highest Q^2 regions.

We conclude from this model study that HERWIG 5.9 gives the best description of the jet distributions measured. At this stage, ARIADNE and LEPTO are unable to describe the data.

6 NLO predictions and determination of α_s

In this section, the jet distribution are compared with perturbative QCD calculations in NLO. In order to obtain a reliable NLO prediction, the restrictive dijet event samples two and three with jets of $\langle E_T^{Breit} \rangle \sim$ 10 GeV are selected for the comparison. The hadronization corrections have been estimated as described in section 4.3 and are applied to the NLO calculations.

6.1 NLO QCD programs

The NLO predictions are calculated with the program DISENT [19]. DISENT allows arbitrary jet definitions and the application of cuts in terms of parton four–momenta. It uses the 'subtraction' method [21] in combination with dipole factorization theorems [22] in order to deal with final–state infrared and collinear divergences associated with real emissions of partons.

Currently four NLO programs are available, DISENT, DISASTER++ [23], JETVIP [24] and MEPJET [25]. Systematic differences between MEPJET and DISENT have been reported [2, 23]. Consequently systematic studies of the four programs were performed in [26] to resolve these ambiguities. An excellent agreement between jet cross sections calculated by DISENT and DISASTER++ is found. Here, DISENT is taken to calculate the NLO distributions.

The statistical precision of the NLO predictions shown below is estimated to be 1–2%.

6.2 Comparison of measured jet distributions with NLO predictions

Before extracting a value of α_s from a comparison of data and NLO calculations, we compare the corrected jet distributions with the NLO predictions for the five observables y_2, θ_{fwd}, θ_{bwd}, z_p and x_p in any of the three Q^2 regions. In the calculation shown in the figures below the parton density functions of CTEQ5M [27], $\Lambda_{\overline{MS}}^{(4)}$ = 330 MeV, and the renormalization scale $\mu_R^2 = Q^2$ are chosen. Note that we use $\Lambda_{\overline{MS}}^{(4)}$ (the (4) stands for the number of flavours) as a technical steering parameter in DISENT. The number of active flavours used in the calculation is set at five. The NLO distributions are multiplied by the hadronization corrections as described above.

In Figure 5 the corrected y_2 distributions measured with the factorizable k_T algorithm are shown together with the NLO prediction plus the hadronization correction. The description of the data is good. In the lowest Q^2 bin the data distribution is slightly higher than the NLO prediction. This difference disappears with increasing Q^2 and a good description of the data is observed in the highest Q^2 range. In all three Q^2 ranges the shape of the measured y_2 distribution is well reproduced. The description of the other variables is also good. This is shown in Figure 6 for the full Q^2 range. The data distributions are slightly higher than the NLO calculations due to the influence of the lowest Q^2 bin.

A good description of the data is also observed for the jet distributions measured with the modified Durham algorithm. The y_2 distribution is shown in Figure 7. The other jet distributions are shown in Figure 8. The distributions of all variables measured with the modified Durham algorithm and with the factorizable k_T algorithm are quite similar. There are small differences, e.g. the angular distributions are slightly shifted to lower angles for the modified Durham algorithm. These differences are well modeled by the NLO calculation. Note the different definition of y_2 for the two algorithms which makes the comparison of this variable less transparent.

From these comparisons we conclude that for the given jet hardness cuts, perturbative QCD in NLO describes the data well in any part of a broad jet phase space region and within a large range of Q^2. This observation does not depend on the particular jet algorithm chosen but is valid for the two complementary jet algorithms that we selected. It is thus possible to proceed with a quantitative determination of the strong coupling constant α_s.

6.3 Fit of α_s

In order to extract α_s, we perform a minimum χ^2 fit of the corrected y_2 distribution and the NLO predictions as a function of $\Lambda^{(4)}_{\overline{MS}}$. In the fit, the y_2 distribution as predicted by QCD in NLO needs to be available for arbitrary values of $\Lambda^{(4)}_{\overline{MS}}$. Thus for each bin in y_2, a precise parameterization of $1/\sigma_{DIS}\ d\sigma_{dijet}/dy_2$ is obtained by an expansion of the form $A(y_2)\,\alpha_s + B(y_2)\,\alpha_s^2$, where α_s is a function of $\Lambda^{(4)}_{\overline{MS}}$. Given A and B and the relation of $\Lambda^{(4)}_{\overline{MS}}$ to α_s, the NLO y_2 distribution can conveniently be calculated for any value of $\Lambda^{(4)}_{\overline{MS}}$.

The coefficients A and B are determined by solving a quadratic equation for each bin in y_2 using the y_2 distributions calculated with DISENT for two values of $\Lambda^{(4)}_{\overline{MS}}$ (300 and 500 MeV). The agreement of this parameterization with direct DISENT calculations was tested for several $\Lambda^{(4)}_{\overline{MS}}$ values between 200 and 600 MeV and was found to be better than a fraction of a percent typically.

In order to relate the fitted value of $\Lambda^{(4)}_{\overline{MS}}$ to $\Lambda^{(5)}_{\overline{MS}}$ and thus to α_s at a given scale μ^2, we use the following formulae [28, 29]

$$\Lambda^{(5)}_{\overline{MS}} = \Lambda^{(4)}_{\overline{MS}}\ (\Lambda^{(4)}_{\overline{MS}}/m_b)^{2/23} \left[\ln(m_b^2/\Lambda^{(4)\,2}_{\overline{MS}})\right]^{-963/13225}, \tag{1}$$

with m_b, the mass of the bottom quark, set to 5 GeV, and

$$\alpha_s(\mu^2) = \frac{4\pi}{\beta_0\ \ln(\mu^2/\Lambda^{(n_f)\,2}_{\overline{MS}})} \left[1 - \frac{2\beta_1}{\beta_0^2}\ \frac{\ln\ln(\mu^2/\Lambda^{(n_f)\,2}_{\overline{MS}})}{\ln(\mu^2/\Lambda^{(n_f)\,2}_{\overline{MS}})}\right], \tag{2}$$

with $\beta_0 = 11 - \frac{2}{3}\,n_f$ and $\beta_1 = 51 - \frac{19}{3}\,n_f$, and n_f the number of quarks of mass less than μ, namely n_f = 5 in our case. We use the same formulae in the DISENT program.

7 Determination of systematic errors

There are several sources of systematic uncertainties that might influence the extracted value of α_s. The size of the effects of the dominant error sources in $\alpha_s(M_Z^2)$ is shown in Figures 9, 10, 11 and 14. The determination of the error is discussed in detail in the three subsections below where the highest Q^2 bin of the jet sample three, based on the factorizable k_T algorithm, is always taken as an example (see Figure 11).

7.1 Experimental errors

Energy calibration
The uncertainty of the hadronic energy scale of the liquid argon calorimeter is $\pm 4\%$ which leads to a systematic shift in the steeply falling y_2 distribution and thus to a variation of $+0.0048$ and -0.0058 in α_s. The hadronic energy scale is the largest source of experimental error.

The uncertainty of the electromagnetic energy scale is $\pm 3\%$. This leads to a variation of $+0.0011$ and -0.0040 in α_s. The corresponding uncertainties for the Durham algorithm are $+0.0014$ and -0.0015. They are smaller since the Durham algorithm is applied in the laboratory frame.

Correction for detector effects and QED radiation
The detector effects and the effects of QED radiation on the measured y_2 distribution are estimated as described in section 4.4. These resulting uncertainty in α_s is $+0.0023$ and -0.0021.

The errors due to the hadronic and electromagnetic energy scale uncertainties, the error due to the model uncertainty of the detector and QED radiation corrections, and the statistical error are added in quadrature to give the combined *experimental* error which is quoted in the Figures 9, 10, 11, 14 and in the Table 2 below.

7.2 Theoretical uncertainties

Hadronization correction

Hadronization is a non-perturbative QCD effect and is understood in terms of phenomenological models only. We observe (see section 4.4) that the spread of the correction factors between the five models is much smaller than the size of the hadronization correction for the y_2 distribution. In order to obtain a realistic error estimate, the uncertainty of the hadronization correction is assumed to be half of the size of the correction factor. This results in a variation of $+0.0026$ and -0.0026 in $\alpha_s(M_Z^2)$.

Renormalization scale
Due to the truncation of the perturbative series in any fixed order calculation, the y_2 distribution depends on the choice of the renormalization scale μ_R^2.

Two possible choices of renormalization scale μ_R^2 are investigated: the photon virtuality Q^2 and the average transverse energy of the two jets squared $\langle E_T^{Breit} \rangle^2$. The latter scale is frequently considered as the more 'natural' choice. Both scales lead to a very good description of the data distributions by the NLO calculation, and lead to similar fit values of α_s. In order to estimate the renormalization scale dependence, μ_R^2 is varied from Q^2 to $Q^2/4$ and $4\ Q^2$ in DISENT and the α_s fit is repeated. The same is done setting $\mu_R^2 = \langle E_T^{Breit} \rangle^2$. The resulting variation of α_s is shown in Table 1. For both choices of μ_R^2, the size of the estimated uncertainty decreases with increasing Q^2. The uncertainty is smaller for $\mu_R^2 = \langle E_T^{Breit} \rangle^2$ than for $\mu_R^2 = Q^2$.

Q^2 range	$\mu_R^2 = Q^2$	$\mu_R^2 = \langle E_T^{Breit} \rangle^2$
$150 < Q^2 < 275$ GeV^2	$+0.0071$ -0.0053	$+0.0060$ -0.0064
$275 < Q^2 < 575$ GeV^2	$+0.0058$ -0.0042	$+0.0036$ -0.0033
$575 < Q^2 < 5000$ GeV^2	$+0.0053$ -0.0038	$+0.0025$ -0.0007

Table 1: Changes of $\alpha_s(M_Z^2)$ when varying the renormalization scales Q^2 and $\langle E_T^{Breit} \rangle^2$ by a factor 1/4 and 4 from the central choice of $\mu_R^2 = Q^2$ and $\langle E_T^{Breit} \rangle^2$, respectively. The numbers are given for the jet sample three, based on the factorizable k_T algorithm.

Here, the larger errors estimated from the variation of $\mu_R^2 = Q^2$ are conservatively taken as the renormalization scale uncertainty, and our central fit value of α_s also assumes $\mu_R^2 = Q^2$. The size of the renormalization scale uncertainty belongs to the dominant error sources.

Factorization scale
In deep–inelastic scattering, collinear initial–state divergences are absorbed into redefined parton densities introducing the dependence on a factorization scale μ_F^2. The value of μ_F^2 has very little influence on the result of this analysis. It was varied from Q^2 to $Q^2/4$ and 4 Q^2. The corresponding effect in $\alpha_s(M_Z^2)$ is less than ± 0.001.

The error due to the uncertainties of the hadronization corrections and the choice of the renormalization scale is added in quadrature to give the combined *theoretical* error.

7.3 Parton density functions

In the NLO calculations, parton density functions are used which have been extracted in global fits to the world data on DIS. Thus experimental measurements performed by experiments other than H1 influence the value of α_s that is determined. Furthermore, the determination of the parton densities depends in general on the choice of the value of the strong coupling constant, α_s^{PDF}, prefered by the authors of the fits. It is important that no bias due to this choice is introduced into this analysis.

In order to study these issues a systematic comparison of essentially all parton density functions that became available during the last years is performed. Thus the fit to the measured y_2 distribution is repeated for the following parton density functions: MRST 1–5 [30, 31]; MRS R1–R4 [32]; the MRS A' series [33]; CTEQ5M and CTEQ5HJ [27]; CTEQ 4A1–4A5

[34]; the CTEQ gluon uncertainty study [35]; CTEQ3 [36]; GRV94HO [15]. Our choice of parton density for the central value of α_s is CTEQ5M which was found to give a good description of the latest H1 structure function measurements [37].

The dependence of our fit result, α_s^{fit}, on the value of the strong coupling in the PDF fits, α_s^{PDF}, is illustrated in Figure 12. For this comparison a subset of the parton densities mentioned above is used. The corresponding series of parton densities (like MRS A' or CTEQ 4A1–4A5) were each determined from the same set of data and with the same fit procedure but for different values of α_s^{PDF}. The figure shows that at $575 < Q^2 < 5000$ GeV^2 only a small correlation of α_s^{PDF} and α_s^{fit} is seen and thus that a significant measurement of α_s can be made. This situation deteriorates at lower Q^2 (not shown) and therefore is investigated in more detail below.

In Figure 13 the dependence of the dijet cross section, σ_{dijet}, and of the inclusive DIS cross section, σ_{DIS}, on α_s^{PDF} is shown for the same subset of parton densities as in the previous figure. The cross sections were obtained from DISENT with $\Lambda^{(4)}_{\overline{MS}}$ = 300 MeV. This compilation is independent of the measurement of the y_2 distribution and of the fit procedure to determine α_s^{fit}. In the lowest Q^2 range the *inclusive DIS* cross section changes significantly with α_s^{PDF} (except for MRST). The *dijet cross* section is essentially independent of α_s^{PDF} for any of the available sets of parton densities. The same feature is observed for the other Q^2 ranges where, however, the effect is less pronounced.

In conclusion, we observe that the dependence of the y_2 distribution, $1/\sigma_{DIS}\ d\sigma_{dijet}/dy_2$ on α_s^{PDF} is almost entirely caused by the systematic correlation of σ_{DIS} with α_s^{PDF}. It should be noted that the extreme values of σ_{DIS} predicted by some of the parton density functions at least in the lowest Q^2 range are not compatible with the latest HERA structure function measurements [37].

At this stage, however, the largest and smallest value of α_s extracted for any of the listed parton density functions and thus for any choice of α_s^{PDF} is conservatively quoted as the *parton density (PDF)* error.

8 Discussion of results

The values of $\alpha_s(M_Z)$ extracted from the fits to the y_2 distribution as measured with the factorizable k_T algorithms are compiled in Table 2. The best precision is reached in the range of largest Q^2.

Consistent and similar results are also obtained with the modified Durham algorithm. This is illustrated in Figure 14, where the value and systematic uncertainties of α_s extracted from the y_2 distribution as measured with the modified Durham algorithm are shown for the range of largest Q^2.

Given the three bins of Q^2, the running of the strong coupling constant as a function of the renormalization scale can be determined. The mean values of Q^2 in the three bins are 210, 380 and 1190 GeV^2, respectively. The corresponding values of α_s, calculated from the $\Lambda^{(4)}_{\overline{MS}}$ fitted in each Q^2 bin using the formulae (1) and (2), are shown in Figure 15. The errors bands in

Q^2 range	$\alpha_s(M_Z^2)$	$\Delta\alpha_s$ (exp.)	$\Delta\alpha_s$ (theor.)	$\Delta\alpha_s$ (PDF)
$150 < Q^2 < 275$ GeV^2	0.1272	$+0.0097$ -0.0063	$+0.0090$ -0.0078	$+0.0042$ -0.0069
$275 < Q^2 < 575$ GeV^2	0.1225	$+0.0110$ -0.0090	$+0.0072$ -0.0061	$+0.0032$ -0.0064
$575 < Q^2 < 5000$ GeV^2	0.1189	$+0.0064$ -0.0081	$+0.0059$ -0.0046	$+0.0013$ -0.0055
$575 < Q^2 < 5000$ GeV^2	0.1143	$+0.0075$ -0.0089	$+0.0074$ -0.0064	$+0.0008$ -0.0054

Table 2: Values of $\alpha_s(M_Z^2)$ determined with the factorizable k_T algorithm in the three different Q^2 ranges (upper three rows). Value of $\alpha_s(M_Z^2)$ determined with the modified Durham algorithm in the range $575 < Q^2 < 5000$ GeV^2 (bottom row).

the bottom part of the figure correspond to correlated errors which would not effect the running of the strong coupling but lead to a global shift of $\alpha_s(Q^2)$ for each Q^2. The measurement is well compatible with the expectation from the renormalization group equation calculated from equation (2) for $\alpha_s(M_Z^2) = 0.119$ (given by the full line).

In a similar way the running of α_s as a function of $\langle E_T^{Breit}\rangle^2$ is shown in Figure 16. Here, the strong correlation of y_2 and $\langle E_T^{Breit}\rangle^2$ is exploited. The value of $\langle E_T^{Breit}\rangle^2$ rises with increasing y_2. The average values of $\langle E_T^{Breit}\rangle^2$ corresponding to the four bins of the y_2 distribution in the range $Q^2 > 150$ GeV^2 are 86, 153, 281 and 553 GeV^2. Thus the running can be tested for lower values of renormalization scales than before. For this comparison, the renormalization scale $\langle E_T^{Breit}\rangle^2$ and not Q^2 was chosen in the NLO calculations. Again, the measured $\alpha_s(\langle E_T^{Breit}\rangle^2)$ is well compatible with the expected running of α_s. Given the size of the errors no significant test of the expected functional form of $\alpha_s(\mu_R^2)$ can yet be made for any of the scales Q^2 or $\langle E_T^{Breit}\rangle^2$.

9 Comparison with an α_s determination from the inclusive jet cross section

In a recent preliminary analysis [38] the H1 Collaboration have also measured the inclusive (single) jet cross section applying the inclusive k_T algorithm [39] in the region of $150 < Q^2 < 5000$ GeV^2 and for transverse jet energies in the Breit frame of $49 < E_T^2 < 2500$ GeV^2. As in this analysis, perturbative QCD calculations in NLO give a good description of the data. The value of the strong coupling constant has been determined for the two choices of renormalization scale $\mu_R^2 = E_T^2$ and Q^2. The results are shown in Figure 17 and 18 together with the results of this analysis. The results of both analyses have been compared and are found to be consistent.

10 Summary

A new measurement of differential dijet distributions in deep–inelastic scattering processes at HERA in the kinematic range $Q^2 > 150$ GeV^2 has been presented. The measurement is based on an integrated luminosity of ~ 35 pb^{-1} which corresponds to an increase of the collected data sample by a factor of ~ 5 in comparison with previous jet measurements [2, 3].

A complete coverage of the jet phase space is provided by measuring distributions of the jet observables y_2, θ_{fwd}, θ_{bwd}, z_p and x_p. The large data sample enables us to study the Q^2 dependences of the jet distributions with high precision. Furthermore the application of severe jet hardness cuts is made possible which gives access to the rare events with pronounced jet structures.

In the first part of this analysis, the quality of the data description by different versions of the Monte Carlo models ARIADNE, LEPTO and HERWIG is investigated. The jet distributions are measured using the modified Durham algorithm which is used for the first time in DIS in this analysis. The parameters of LEPTO were varied to optimize the description of the measured jet distributions. The models ARIADNE and LEPTO are, however, unable to describe all features of the jet distributions. The best description of the data is obtained with HERWIG.

In the second part of this analysis, a systematic comparison with perturbative QCD predictions in NLO is performed. Two jet algorithms with different properties, the modified Durham and the factorizable k_T algorithm, are used. Event samples with hard dijets of a mean transverse jet energy in the Breit frame, $\langle E_T^{Breit} \rangle$, of ~ 10 GeV are selected. Again a complete set of jet variables is measured for any of the two algorithms. The data are well described by perturbative QCD calculations in NLO combined with hadronization corrections estimated with Monte Carlo models.

A measurement of the value of α_s is performed in three bins of Q^2. The size of the systematic uncertainties is smallest at high Q^2. In the range $575 < Q^2 < 5000$ GeV^2 we obtain

$$\alpha_s(M_Z^2) = 0.1189^{+0.0064}_{-0.0081}\,(exp.)\,^{+0.0059}_{-0.0046}\,(theor.)\,^{+0.0013}_{-0.0055}\,(PDF)$$

for the factorizable k_T algorithm and

$$\alpha_s(M_Z^2) = 0.1143^{+0.0075}_{-0.0089}\,(exp.)\,^{+0.0074}_{-0.0064}\,(theor.)\,^{+0.0008}_{-0.0054}\,(PDF)$$

for the modified Durham algorithm. Both results agree well with each other.

The running of the strong coupling constant is determined as a function of the renormalization scale $\mu_R^2 = Q^2$ and $\langle E_T^{Breit} \rangle^2$. Both choices of the renormalization scale lead to a good description of the data, and for both choices the dependence of the strong coupling on the renormalization scale is as expected by QCD. These results are similar to and consistent with those of the preliminary H1 analysis of [38].

Acknowledgements

We are very grateful to the HERA machine group whose outstanding efforts made this experiment possible. We acknowledge the support of the DESY technical staff. We appreciate the big effort of the engineers and technicians who constructed and maintain the detector. We thank the funding agencies for financial support of this experiment. We wish to thank the DESY directorate for the support and hospitality extended to the non–DESY members of the collaboration.

References

[1] H1 Collaboration, T. Ahmed et *al.*, Phys. Lett. **B346** (1995) 415;
ZEUS Collaboration, M. Derrick et *al.*, Phys. Lett. **B363** (1995) 201.

[2] H1 Collaboration, C. Adloff et *al.*, Eur. Phys. J. **C6** (1999) 4, 575.

[3] H1 Collaboration, C. Adloff et *al.*, Eur. Phys. J. **C5** (1998) 4, 625.

[4] JADE Collaboration, W. Bartel et *al.*, Z. Phys. **C33** (1986) 23;
JADE Collaboration, S. Bethke et *al.*, Phys. Lett. **B213** (1988) 235.

[5] S. Catani, Yu.L. Dokshitzer, B.R. Webber, Phys. Lett **B285** (1992) 291.

[6] G. Ingelman, LEPTO, version 6.1, Proc. of the Workshop '*Physics at HERA*', Eds. W. Buchmüller and G. Ingelman, Vol. 3 (1992) 1366;
G. Ingelman, A. Edin and J. Rathsman, Comp. Phys. Comm. **101** (1997) 108.

[7] L. Lönnblad, Comp. Phys. Comm. **71** (1992) 15.

[8] See proceedings of the Workshop on *Monte Carlo Generators for HERA Physics'*, Eds. T. Doyle, G. Grindhammer, G. Ingelmann and H. Jung, DESY (1999), to be published.

[9] G. Marchesini et *al.*, Comput. Phys. Commun. **67** (1992), 465.

[10] H1 Collaboration, I. Abt et *al.*, Nucl. Instr. and Meth. **A386** (1997) 310 and 348.

[11] H1 Calorimeter Group, B. Andrieu et *al.*, Nucl. Instr. and Meth. **A336** (1993) 499;
H1 Calorimeter Group, B. Andrieu et *al.*, Nucl. Instr. and Meth. **A350** (1994) 57.

[12] S. Bentvelsen et *al.*, Proc. of the Workshop '*Physics at HERA*', Eds. W. Buchmüller and G. Ingelman, Vol. 1 (1991) 23;
K.C. Höger, ibid. 43.

[13] DJANGO 6.2; G.A. Schuler and H. Spiesberger, Proc. of the Workshop '*Physics at HERA*', Eds. W. Buchmüller and G. Ingelman, Vol. 3 (1991) 1419.

[14] V. Blobel, DESY 84–118, Dec. 1984 and Proc. of the 1984 CERN School of Computing, Aiguablava, Spain.

[15] M. Glück, E. Reya and A. Vogt, Z. Phys. **C67** (1995) 433;
M. Glück, E. Reya and A. Vogt, Z. Phys. **C53** (1992) 127.

[16] B. Andersson et *al.*, Phys. Rep. **97** (1983) 31;
T. Sjöstrand and M. Bengtssen, Comp. Phys. Comm. **43** (1987) 367.

[17] J. Rathsman, Phys. Lett. **B452** (1999) 364.

[18] N. Brook et *al.*, Proc. of the Workshop *Future Physics at HERA*, Eds. G. Ingelman, A. de Roeck and R. Klanner, Vol. 1 (1995/96) 614.

[19] S. Catani and M.H. Seymour, Nucl. Phys. **B485** (1997) 291.

[20] B.R. Webber, Nucl. Phys. **B238** (1984) 492.

[21] R.K. Ellis, D.A. Ross and A.E. Terrano, Nucl. Phys. **B178** (1981) 421;
Z. Kunszt and D.E. Soper, Phys. Rev. **D46** (1992) 192.

[22] S. Catani and M.H. Seymour, Phys. Lett. **B378** (1996) 287.

[23] D. Graudenz, hep-ph/9710244.

[24] B. Poetter, preprint DESY-98-71 (1998), hep-ph/9806437.

[25] E. Mirkes and D. Zeppenfeld, Phys. Lett. **B380** (1996) 205.

[26] Report of the working group *Fixed higher order programs for DIS and photoproduction*, Proc. of the Workshop on *Monte Carlo Generators for HERA Physics*, Eds. T. Doyle, G. Grindhammer, G. Ingelmann and H. Jung, DESY (1999), to be published.

[27] CTEQ5 Collaboration, H.L. Lai *al.*, hep-ph/9903282.

[28] W. Marciano, Phys. Rev. **D29** (1984) 580.

[29] Particle Data Group, Phys. Rev. **D54** (1996), 77.

[30] A.D. Martin, R.G. Roberts, W.J. Stirling and R.S. Thorne, Eur. Phys. J. **C4** (1998) 463.

[31] A.D. Martin, R.G. Roberts, W.J. Stirling and R.S. Thorne, hep-ph/9906231.

[32] A.D. Martin, R.G. Roberts and W.J. Stirling, Phys. Lett. **B387** (1996) 419.

[33] A.D. Martin, R.G. Roberts and W.J. Stirling, Phys. Lett. **B356** (1995) 89.

[34] H.L. Lai *al.*, Phys. Rev. **D55** (1997) 1280.

[35] J. Huston *al.*, Phys. Rev. **D58** (1998) 114034.

[36] H.L. Lai *al.*, Phys. Rev. **D51** (1995) 4763.

[37] H1 Collaboration, C. Adloff et *al.*, *Measurement of Neutral and Charged Current Cross Sections in Positron-Proton Collisions at Large Momentum Transfer*, in preparation.

[38] H1 Collaboration, *Determination of the Strong Coupling Constant from the Inclusive Jet Cross Section in Deep-Inelastic Positron-Proton Collisions at HERA*, abstract 157, submitted to this conference.

[39] S.D. Ellis and D.E. Soper, Phys. Rev. **D48** (1993) 3160;
S. Catani, Yu.L. Dokshitzer, M.H. Seymour, B.R. Webber, Nucl. Phys. **B406** (1993) 187.

[40] S. Bethke, Proc. of the IVth Int. Symposium on Radiative Corrections (RADCOR 98), Catalonia, Spain (1998), hep-ex/9812026.

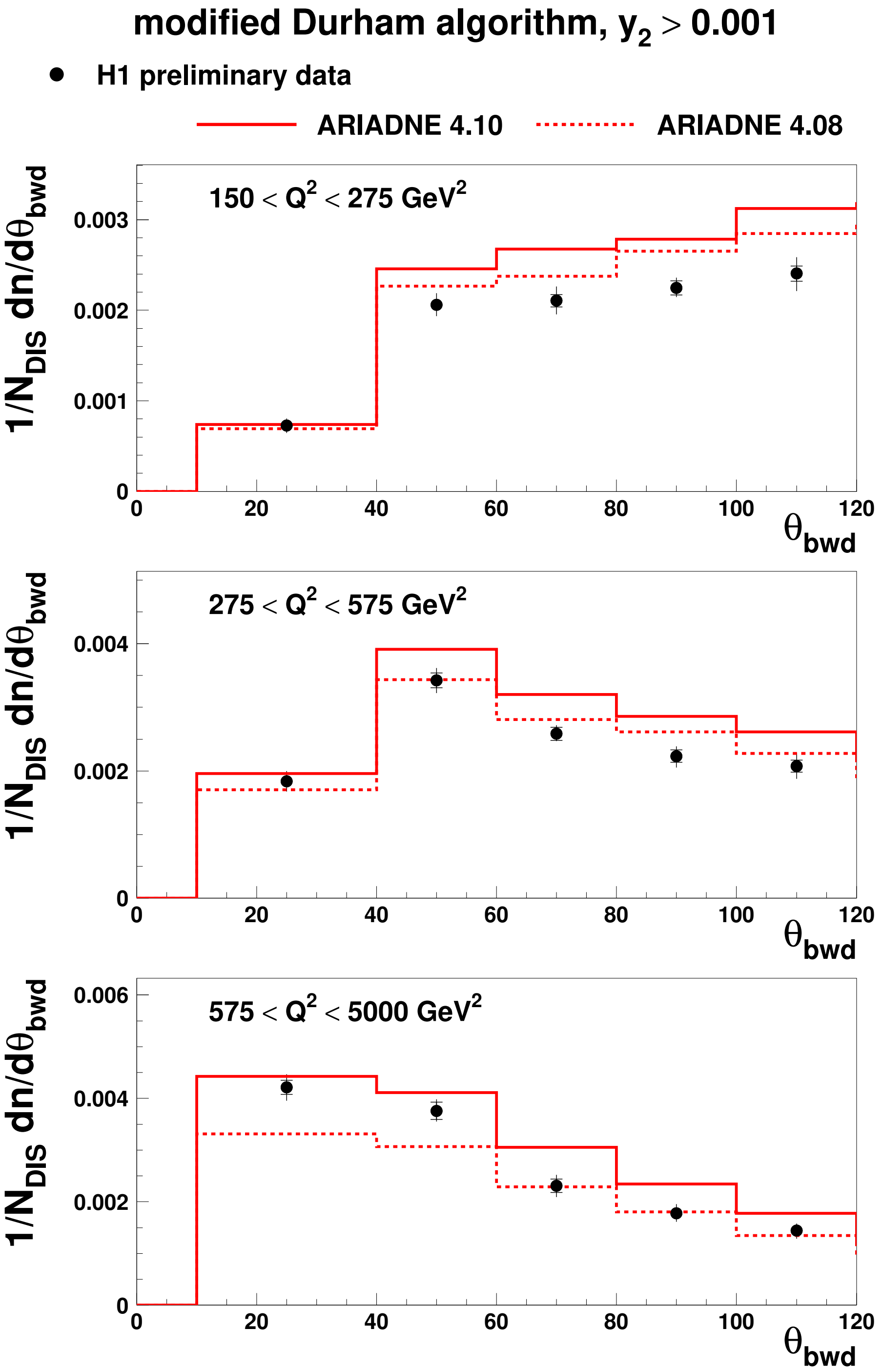

Figure 1: Distribution of θ_{bwd} determined with the modified Durham algorithm for $y_2 = k_T^2/W^2 > 0.001$ and $10° < \theta_{jet} < 140°$. The measured distribution, corrected for detector effects and the effects of QED radiation, is shown for three ranges of Q^2. The inner error bars show the statistical error. The total error bars correspond to the statistical and systematic errors added in quadrature. Also shown are the predictions of the MC model ARIADNE, version 4.10 (full line) and version 4.08 (dashed line).

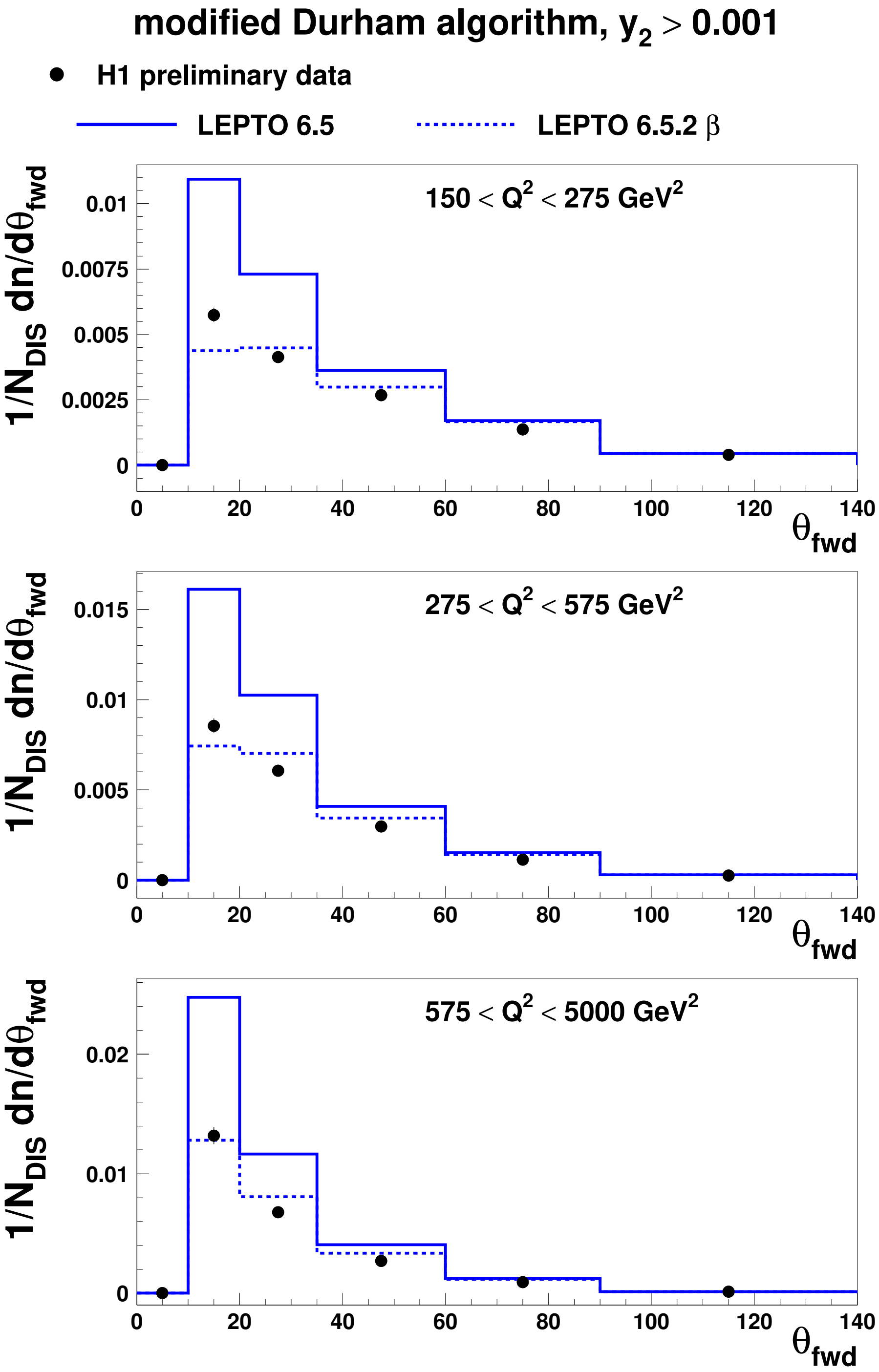

Figure 2: Distribution of θ_{fwd} determined with the modified Durham algorithm for $y_2 = k_T^2/W^2 > 0.001$ and $10° < \theta_{jet} < 140°$. The measured distribution, corrected for detector effects and the effects of QED radiation, is shown for three ranges of Q^2. The inner error bars show the statistical error. The total error bars correspond to the statistical and systematic errors added in quadrature. Also shown are the predictions of the MC model LEPTO, version 6.5 (full line) and version 6.5.2β (dashed line).

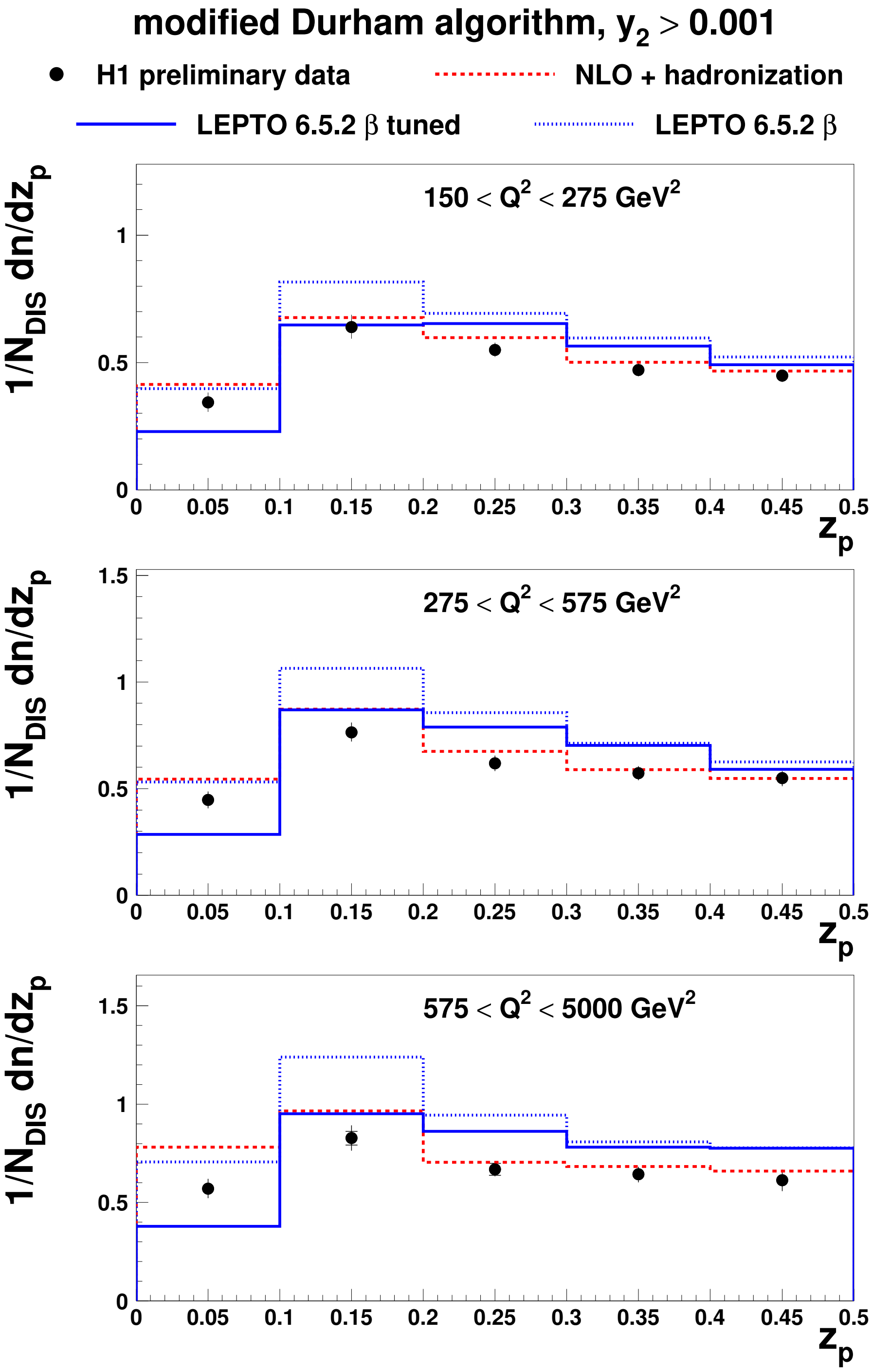

Figure 3: Distribution of z_p determined with the modified Durham algorithm for $y_2 = k_T^2/W^2 > 0.001$ and $10° < \theta_{jet} < 140°$. The measured distribution, corrected for detector effects and the effects of QED radiation, is shown for three ranges of Q^2. The inner error bars show the statistical error. The total error bars correspond to the statistical and systematic errors added in quadrature. Also shown are the predictions of the MC model LEPTO, version 6.5.2β with tuned (full line) and default model parameters (dotted line), and perturbative QCD calculations in NLO (dashed line) based on DISENT. The parton density functions CTEQ5M were used for the calculation in combination with $\Lambda^{(4)}_{\overline{MS}} = 300$ MeV.

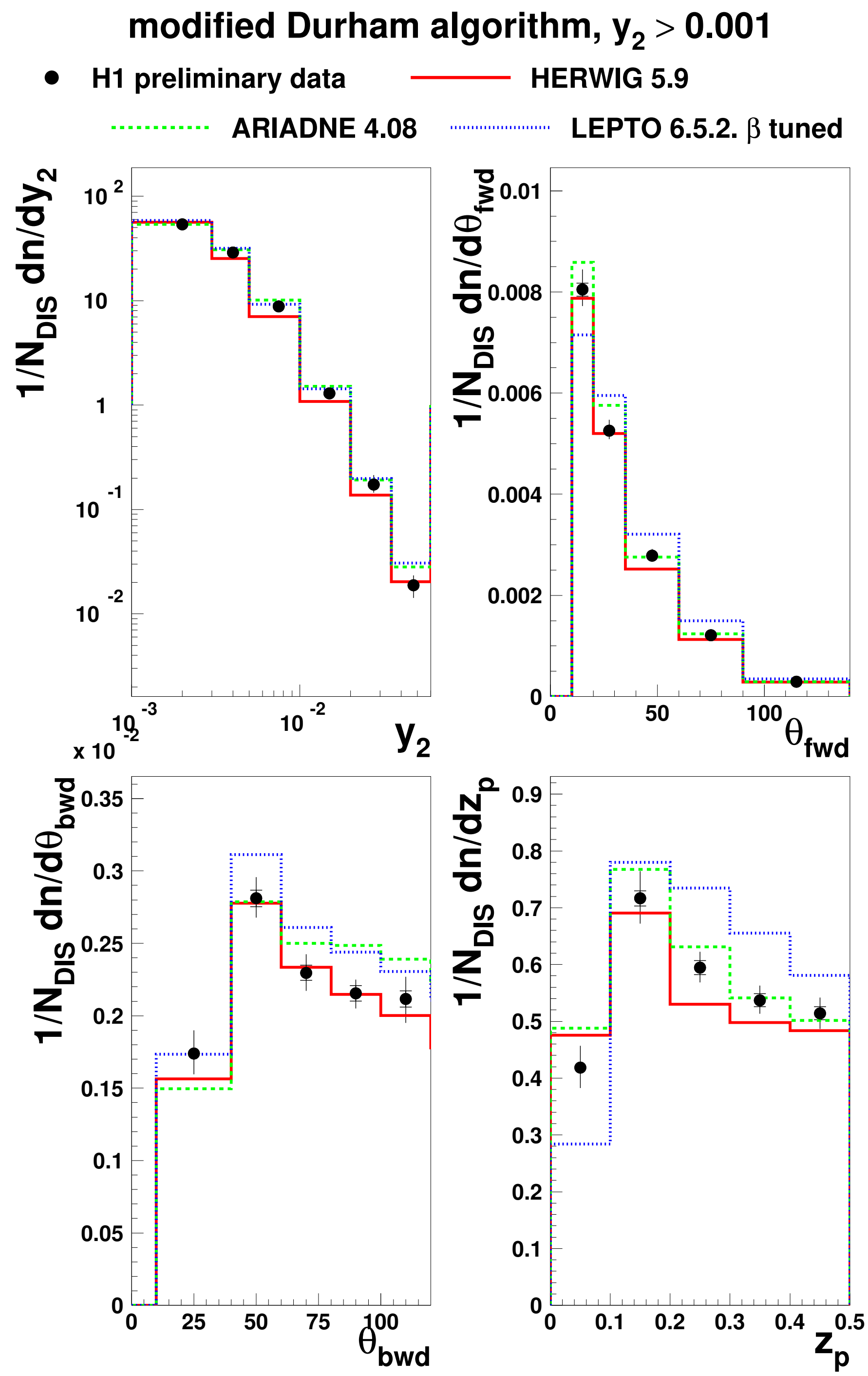

Figure 4: Distribution of y_2, z_p, θ_{fwd} and θ_{bwd} determined with the modified Durham algorithm for $y_2 = k_T^2/W^2 > 0.001$ and $10° < \theta_{jet} < 140°$. The measured distribution, corrected for detector effects and the effects of QED radiation, is shown for the range of $Q^2 > 150$ GeV^2. The inner error bars show the statistical error. The total error bars correspond to the statistical and systematic errors added in quadrature. Also shown are the predictions of the MC model HERWIG (full line), the predictions of LEPTO, version 6.5.2β with tuned model parameters (dotted line) and those of ARIADNE, version 4.08, (dashed line).

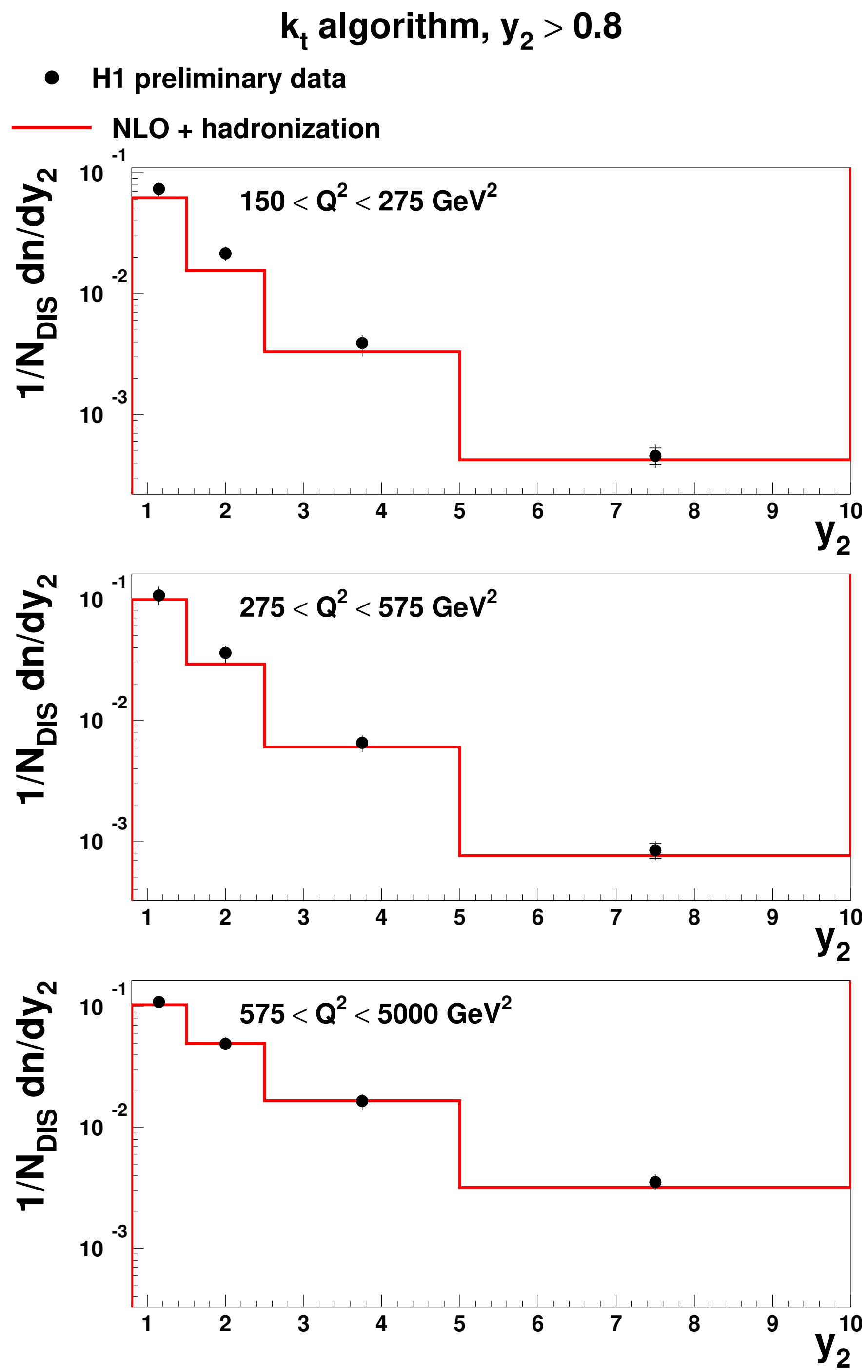

Figure 5: Distribution of $y_2 = k_T^2/100$ (GeV^2) determined with the factorizable k_T algorithm for $y_2 > 0.8$ and $10° < \theta_{jet} < 140°$. The measured distribution, corrected for detector effects and the effects of QED radiation, is shown for three ranges of Q^2. The inner error bars show the statistical error. The total error bars correspond to the statistical and systematic errors added in quadrature. Also shown are perturbative QCD calculations in NLO based on DISENT. The parton density functions CTEQ5M were used for the calculation in combination with $\Lambda_{\overline{MS}}^{(4)} = 330$ MeV.

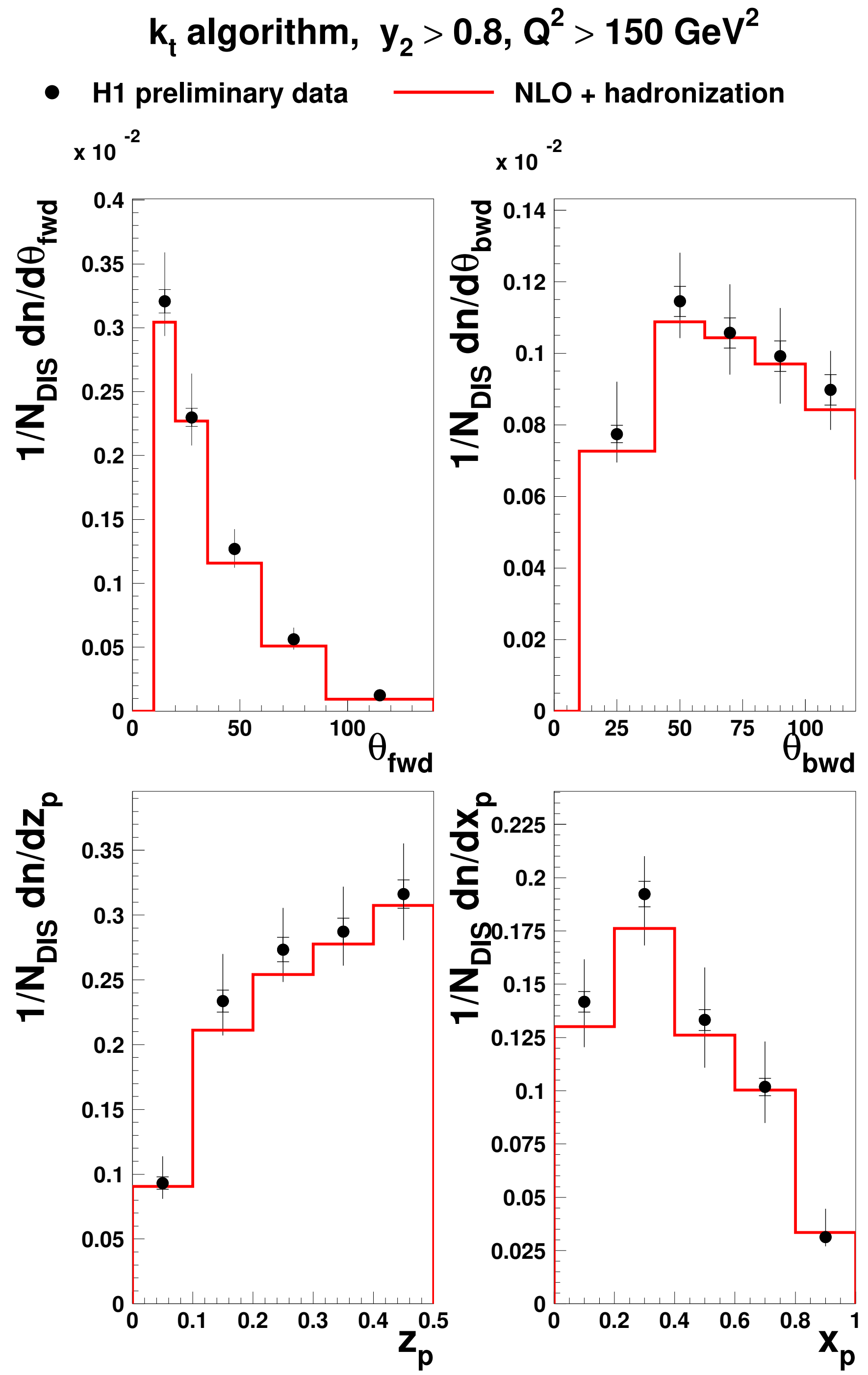

Figure 6: Distribution of θ_{fwd}, θ_{bwd}, z_p and x_p determined with the factorizable k_T algorithm for $y_2 = k_T^2/100\ (\mathrm{GeV}^2) > 0.8$ and $10° < \theta_{jet} < 140°$. The measured distribution, corrected for detector effects and the effects of QED radiation, is shown for the range of $Q^2 > 150$ GeV^2. The inner error bars show the statistical error. The total error bars correspond to the statistical and systematic errors added in quadrature. Also shown are perturbative QCD calculations in NLO based on DISENT. The parton density functions CTEQ5M were used for the calculation in combination with $\Lambda^{(4)}_{\overline{MS}} = 330$ MeV.

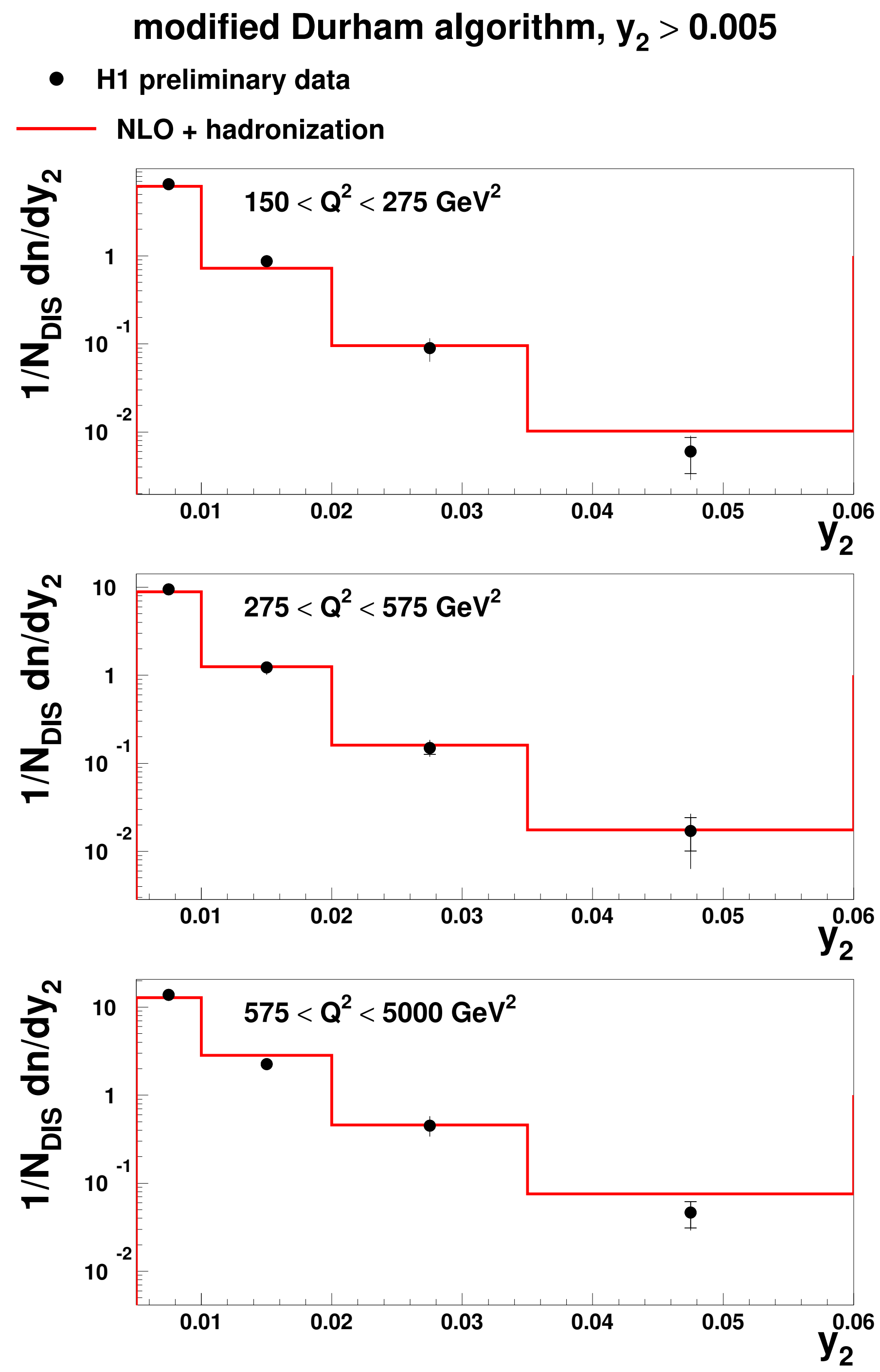

Figure 7: Distribution of $y_2 = k_T^2/W^2$ determined with the modified Durham algorithm for $y_2 > 0.005$ and $10° < \theta_{jet} < 140°$. The measured distribution, corrected for detector effects and the effects of QED radiation, is shown for three ranges of Q^2. The inner error bars show the statistical error. The total error bars correspond to the statistical and systematic errors added in quadrature. Also shown are perturbative QCD calculations in NLO based on DISENT. The parton density functions CTEQ5M were used for the calculation in combination with $\Lambda^{(4)}_{\overline{MS}} = 330$ MeV.

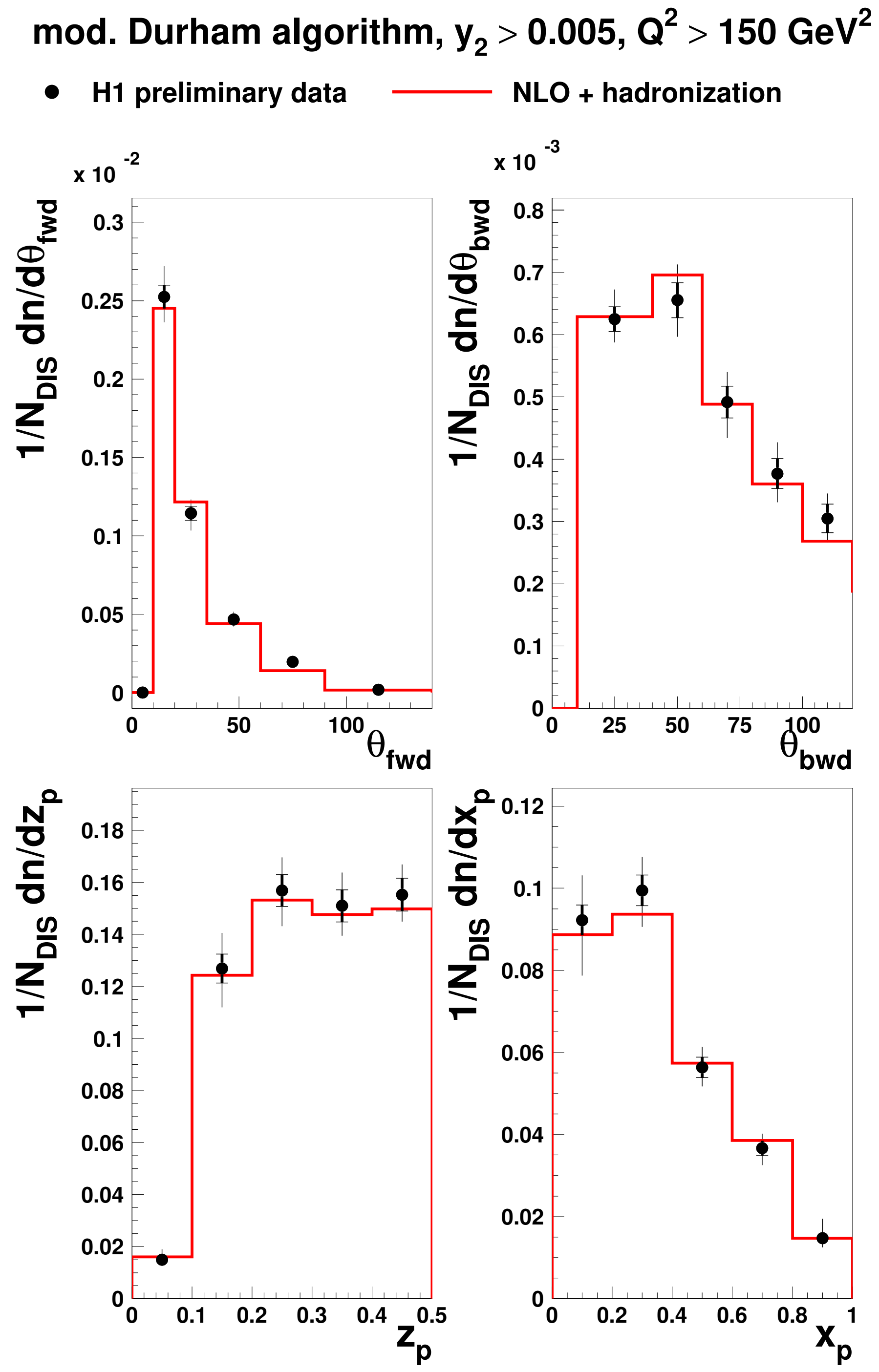

Figure 8: Distribution of θ_{fwd}, θ_{bwd}, z_p and x_p determined with the modified Durham algorithm for $y_2 = k_T^2/W^2 > 0.005$ and $10° < \theta_{jet} < 140°$. The measured distribution, corrected for detector effects and the effects of QED radiation, is shown for the range of $Q^2 > 150$ GeV^2. The inner error bars show the statistical error. The total error bars correspond to the statistical and systematic errors added in quadrature. Also shown are perturbative QCD calculations in NLO based on DISENT. The parton density functions CTEQ5M were used for the calculation in combination with $\Lambda_{\overline{MS}}^{(4)} = 330$ MeV.

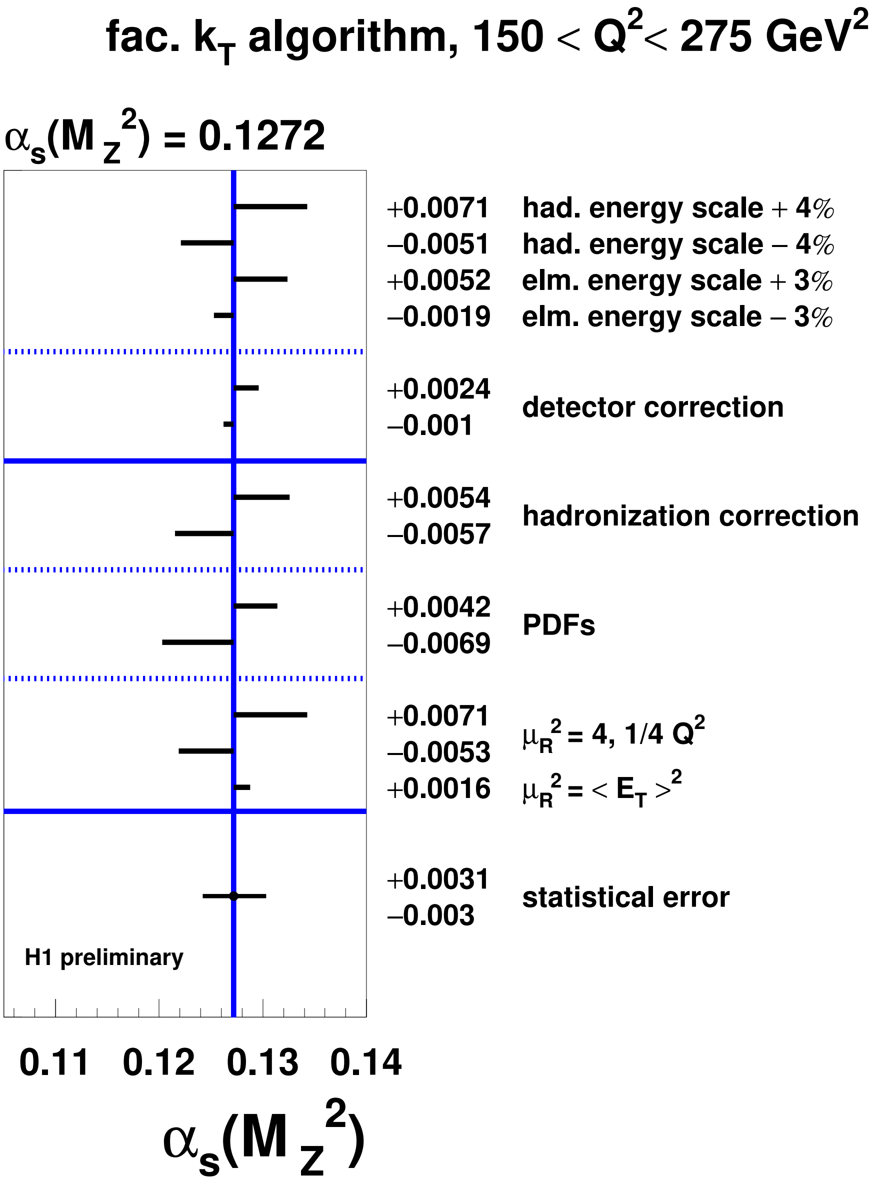

Figure 9: List of systematic uncertainties of the value of α_s fitted to the y_2 distribution measured with the factorizable k_T algorithm in the range $150 < Q^2 < 275$ GeV^2. The horizontal lines separate the different classes of uncertainties. The vertical line indicates the central value of $\alpha_s(M_Z^2)$ resulting from the fit. The black points give the values of α_s that are obtained when each source of systematic error is varied as described in the text. The value of $\alpha_s(M_Z^2)$ is: $0.1272^{+0.0097}_{-0.0063}\,(exp.)\,^{+0.0090}_{-0.0078}\,(theor.)\,^{+0.0042}_{-0.0069}\,(PDF)$.

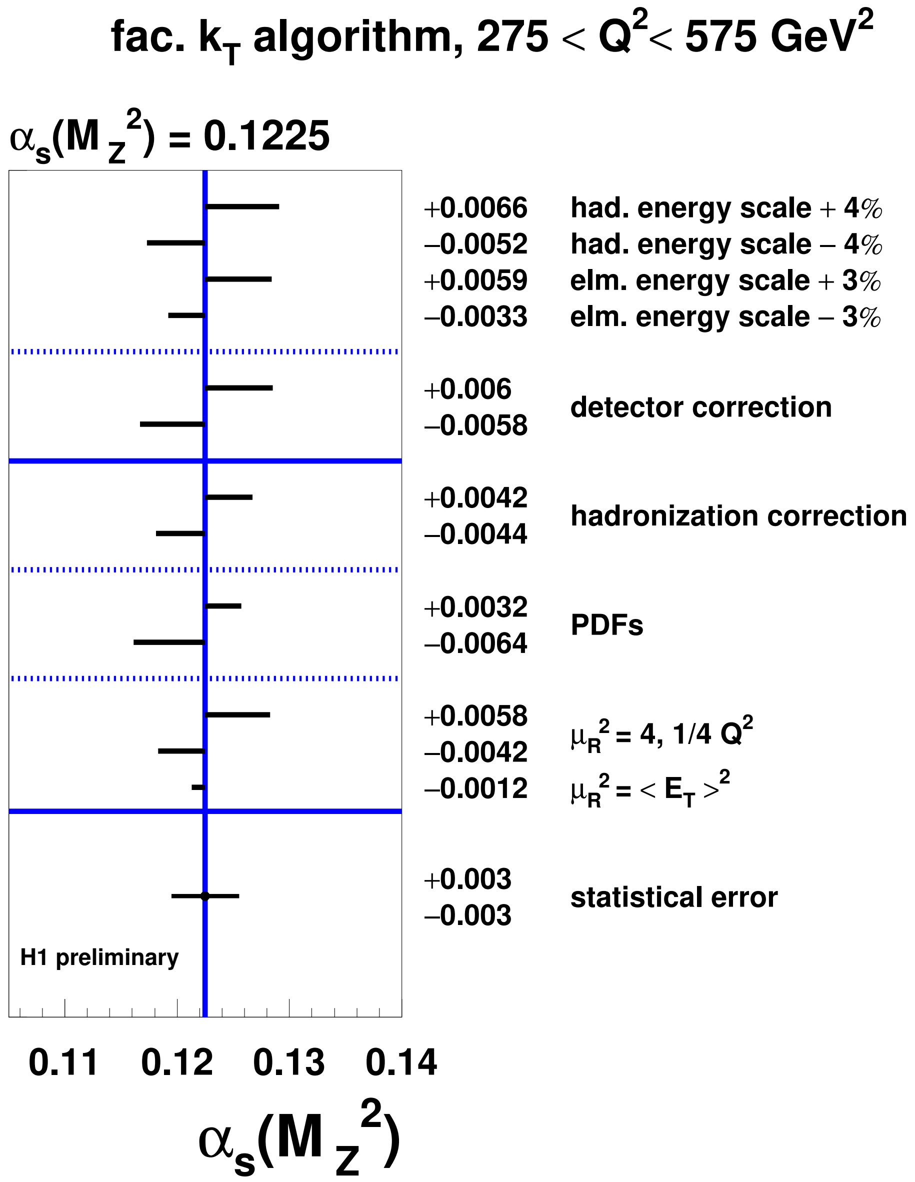

Figure 10: List of systematic uncertainties of the value of α_s fitted to the y_2 distribution measured with the factorizable k_T algorithm in the range $275 < Q^2 < 575$ GeV^2. The horizontal lines separate the different classes of uncertainties. The vertical line indicates the central value of $\alpha_s(M_Z^2)$ resulting from the fit. The black points give the values of α_s that are obtained when each source of systematic error is varied as described in the text. The value of $\alpha_s(M_Z^2)$ is: $0.1225^{+0.0110}_{-0.0090}\,(exp.)\,^{+0.0072}_{-0.0061}\,(theor.)\,^{+0.0032}_{-0.0064}\,(PDF)$.

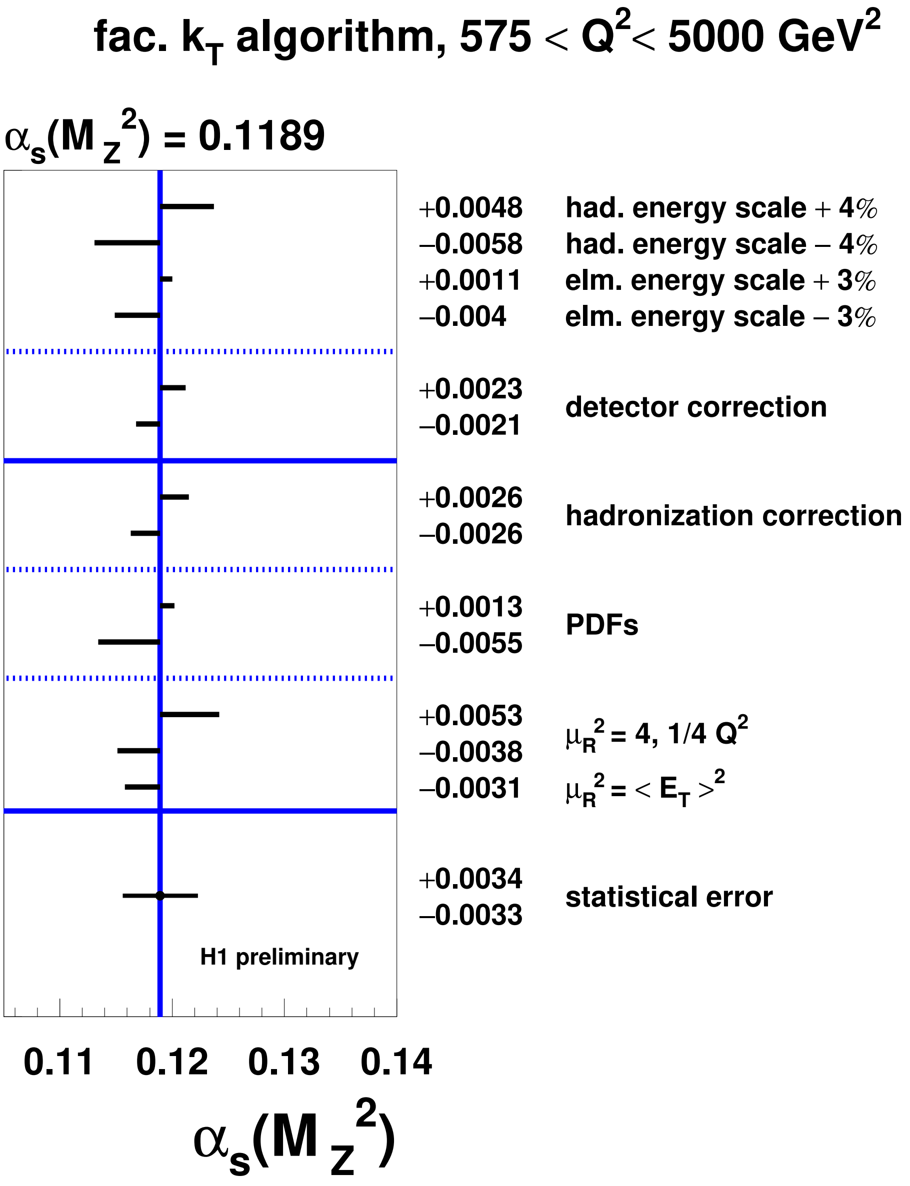

Figure 11: List of systematic uncertainties of the value of α_s fitted to the y_2 distribution measured with the factorizable k_T algorithm in the range $575 < Q^2 < 5000$ GeV^2. The horizontal lines separate the different classes of uncertainties. The vertical line indicates the central value of $\alpha_s(M_Z^2)$ resulting from the fit. The black points give the values of α_s that are obtained when each source of systematic error is varied as described in the text. The value of $\alpha_s(M_Z^2)$ is: $0.1189^{+0.0064}_{-0.0081}\,(exp.)\,^{+0.0059}_{-0.0046}\,(theor.)\,^{+0.0013}_{-0.0055}\,(PDF)$.

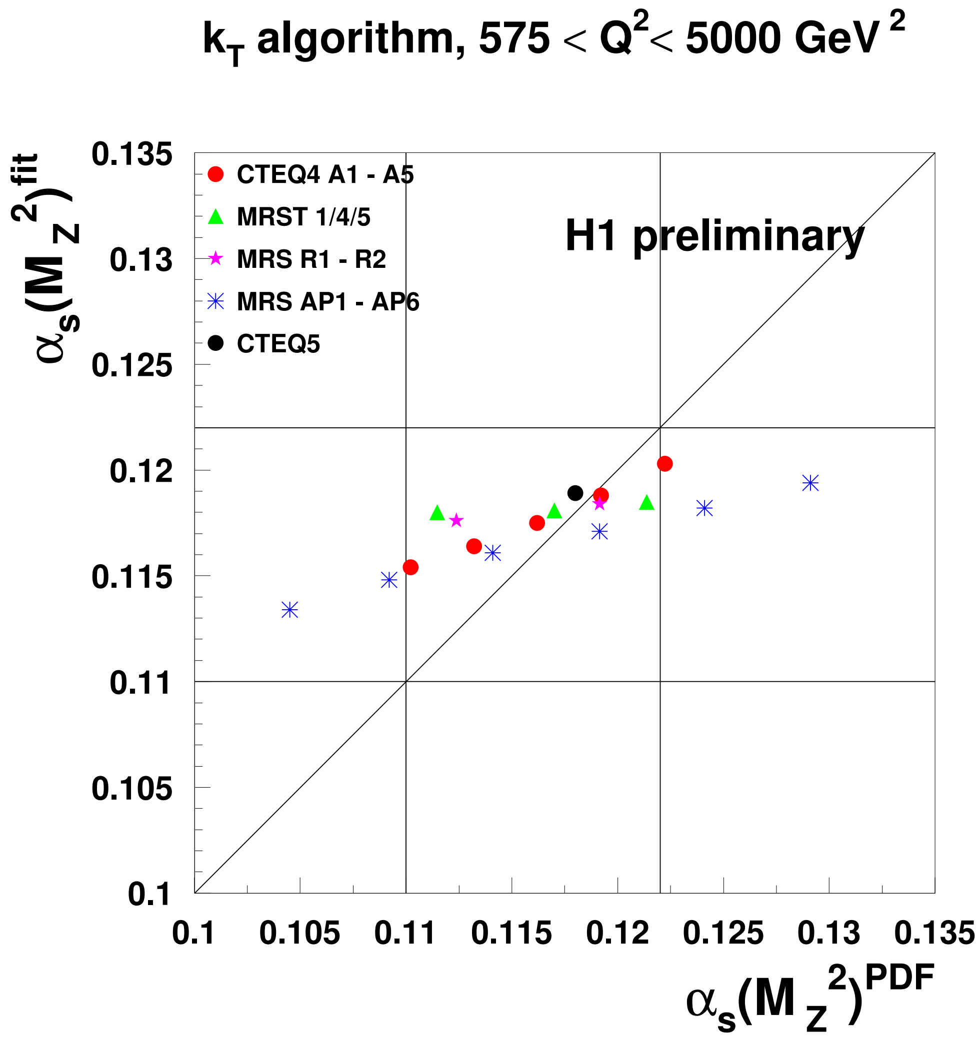

Figure 12: Comparison of $\alpha_s^{fit}(M_Z^2)$ and $\alpha_s^{PDF}(M_Z^2)$ for various choices of parton density functions. The value of α_s^{fit} was fitted in the range of $575 < Q^2 < 5000$ GeV^2 as described in the text; α_s^{PDF} is the value of $\alpha_s(M_Z^2)$ that was used for the parton density extractions from the world data.

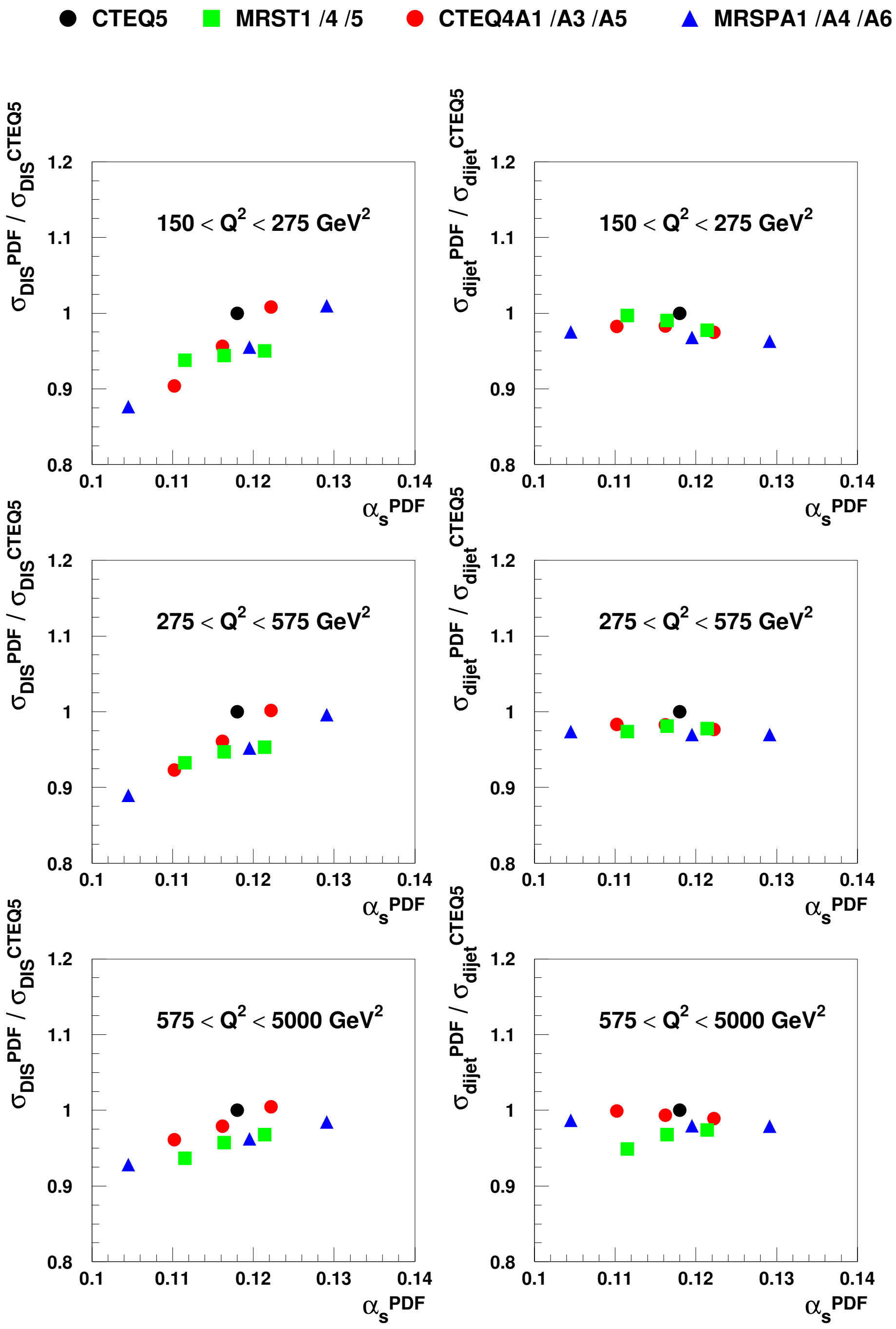

Figure 13: (Left) The variation of the (inclusive) DIS cross section, $\sigma_{\rm DIS}$, versus α_s^{PDF} for various parton density functions. (Right) The corresponding variation of the cross section of the selected jet sample $\sigma_{\rm dijet}$. Both $\sigma_{\rm DIS}$ and $\sigma_{\rm dijet}$ were calculated with DISENT in NLO with $\Lambda^{(4)}_{\overline{MS}}$ fixed to 300 MeV, irrespectively of the value of α_s^{PDF}.

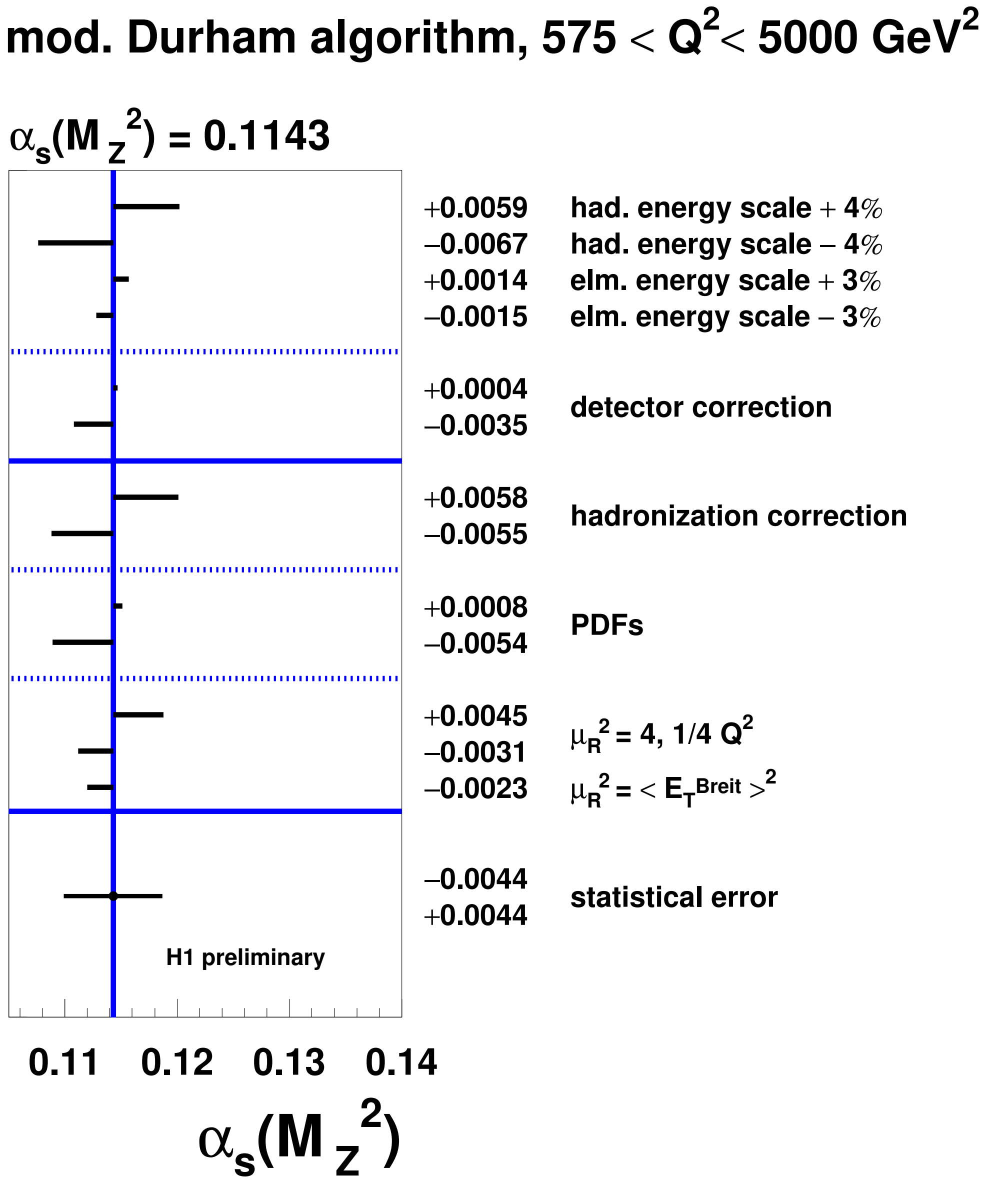

Figure 14: List of systematic uncertainties of the value of α_s fitted to the y_2 distribution measured with the modified Durham algorithm in the range $575 < Q^2 < 5000$ GeV^2. The horizontal lines separate the different classes of uncertainties. The vertical line indicates the central value of $\alpha_s(M_Z^2)$ resulting from the fit. The black points give the values of α_s that are obtained when each source of systematic error is varied as described in the text. The value of $\alpha_s(M_Z^2)$ is: $0.1143^{+0.0075}_{-0.0089}\,(exp.)\,^{+0.0074}_{-0.0064}\,(theor.)\,^{+0.0008}_{-0.0054}\,(PDF)$.

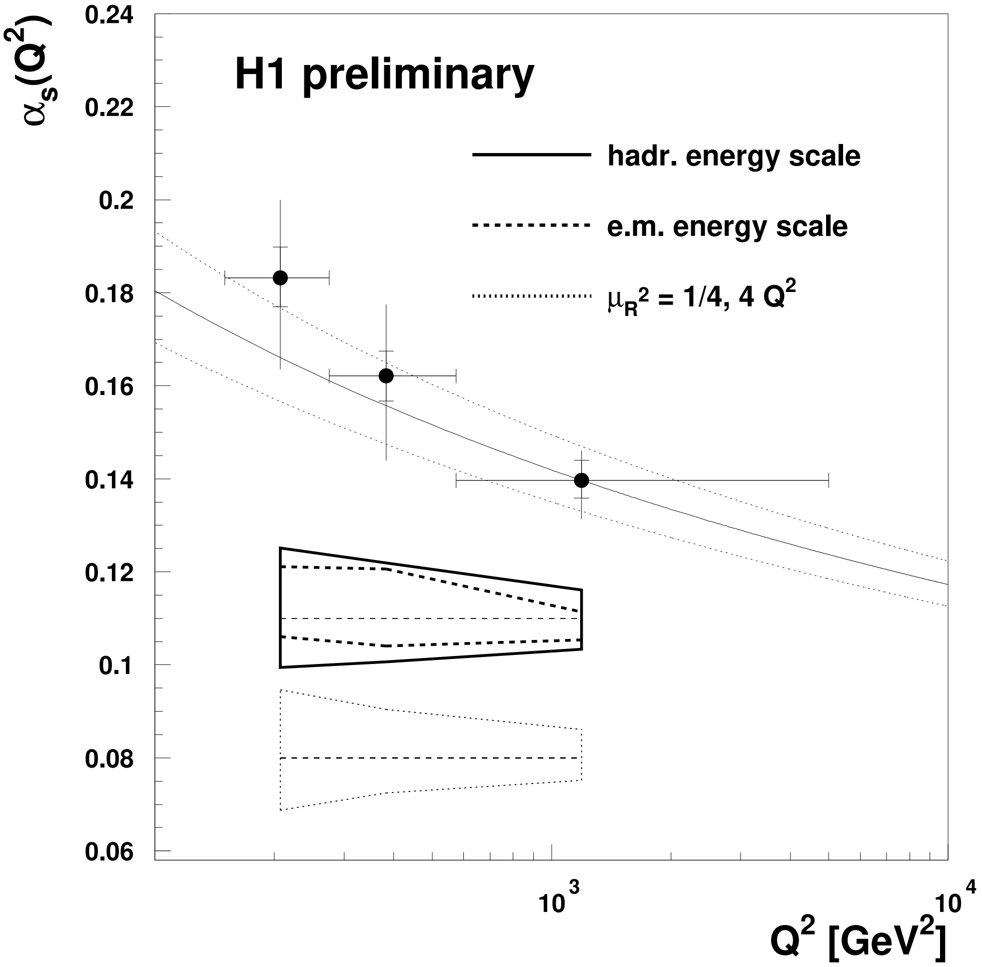

Figure 15: The α_s values determined with the factorizable k_T algorithm in the three Q^2 ranges are shown as a function of the mean value of Q^2 in the given Q^2 range. The total vertical error bars correspond to the statistical error, the error due to the model dependence of the detector correction and the uncertainty due to the variation of the parton density functions added in quadrature. The inner vertical error bars show the statistical error only. The horizontal lines indicate the Q^2 range in which the corresponding α_s value was measured. The full and the dotted curves correspond to the QCD expectation for $\alpha_s(Q^2)$ for the word average value of $\alpha_s(M_Z^2)$ $= 0.119$ and a variation of ± 0.005, respectively. The systematic error due to the uncertainties of the hadronic and electromagnetic energy calibration is shown in the full and dashed error bands. The systematic uncertainty estimated for the renormalization scale uncertainty is shown by the dotted band.

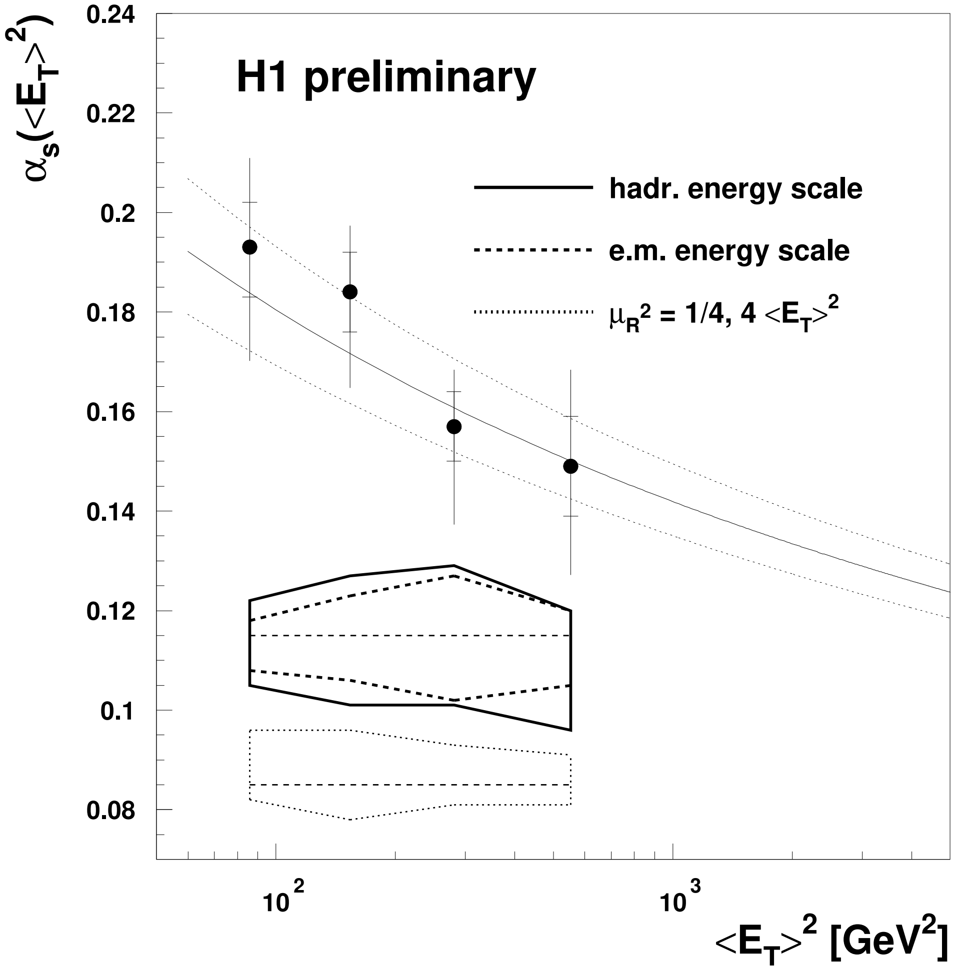

Figure 16: The α_s values determined with the factorizable k_T algorithm for the four y_2 bins in the Q^2 range of $Q^2 > 150$ GeV^2 are shown as a function of the corresponding mean transverse energy squared $< E_T^{Breit} >^2$. The total vertical error bars correspond to the statistical error, the error due to the model dependence of the detector correction and the uncertainty due to the variation of the parton density functions added in quadrature. The inner vertical error bars show the statistical error only. The full and the dotted curves correspond to the QCD expectation for $\alpha_s(Q^2)$ for the word average value of $\alpha_s(M_Z^2) = 0.119$ and a variation of ± 0.005, respectively. The systematic error due to the uncertainties of the hadronic and electromagnetic energy calibration is shown in the full and dashed error bands. The systematic uncertainty estimated for the renormalization scale uncertainty is shown by the dotted band.

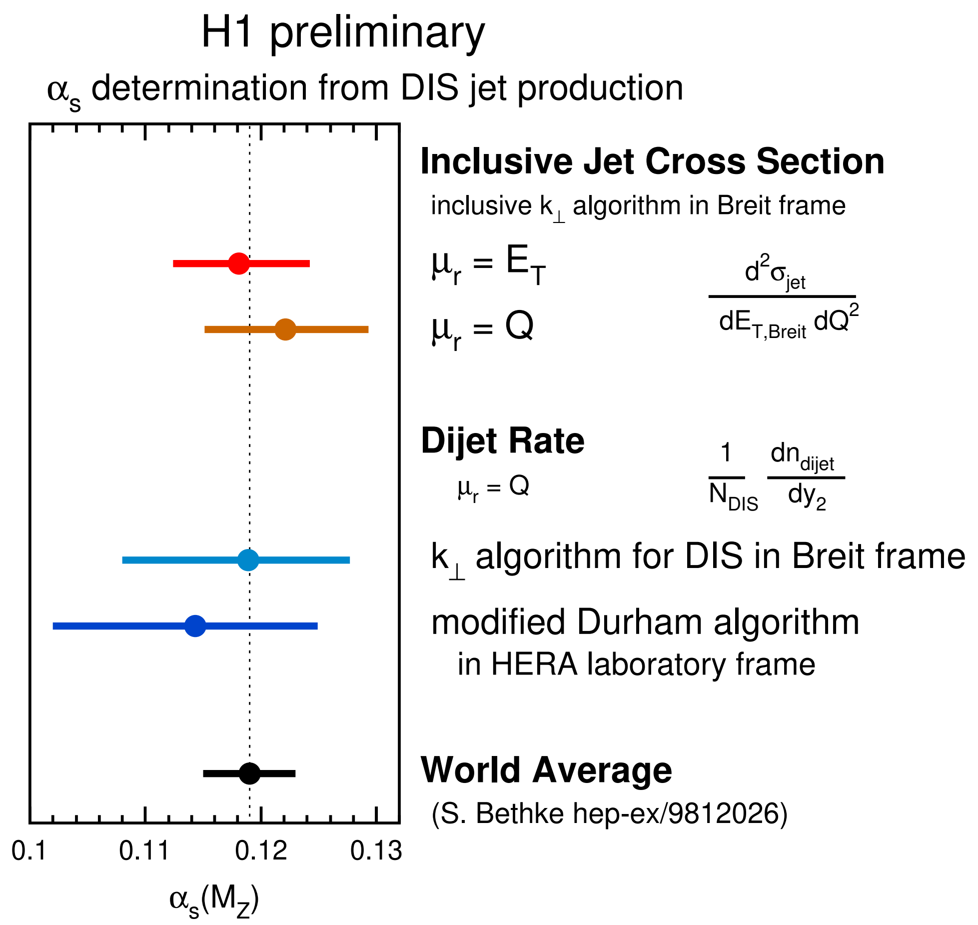

Figure 17: Comparison of the preliminary values of $\alpha_s(M_Z)$ determined from the analysis of the inclusive jet cross section [38] with the present results determined from the measurement of the dijet event rate for the the factorizable k_T and the modified Durham algorithm. Also shown is the current world average value for $\alpha_s(M_Z)$ [40].

H1 preliminary

α_s determination from DIS jet production

Inclusive Jet Cross Section $\quad \dfrac{d^2\sigma_{jet}}{dE_{T,Breit}\, dQ^2}$

inclusive $k_\perp$ algorithm in Breit frame

$\mu_r = E_T$

$\alpha_s(M_Z) = 0.1181 \;\pm 0.0030\ (\mathrm{exp})\ {}^{+0.0039}_{-0.0046}\ (\mathrm{theo})\ {}^{+0.0036}_{-0.0015}\ (\mathrm{pdf})$

$\mu_r = Q$

$\alpha_s(M_Z) = 0.1221 \;\pm 0.0034\ (\mathrm{exp})\ {}^{+0.0054}_{-0.0059}\ (\mathrm{theo})\ {}^{+0.0033}_{-0.0016}\ (\mathrm{pdf})$

Dijet Rate $\quad \dfrac{1}{N_{DIS}} \dfrac{dn_{dijet}}{dy_2}$

$\mu_r = Q$ $\quad k_\perp$ algorithm for DIS in Breit frame

$\alpha_s(M_Z) = 0.1189\ {}^{+0.0064}_{-0.0081}\ (\mathrm{exp})\ {}^{+0.0059}_{-0.0046}\ (\mathrm{theo})\ {}^{+0.0013}_{-0.0055}\ (\mathrm{pdf})$

$\mu_r = Q$ $\quad$ modified Durham algorithm in laboratory frame

$\alpha_s(M_Z) = 0.1143\ {}^{+0.0075}_{-0.0089}\ (\mathrm{exp})\ {}^{+0.0074}_{-0.0064}\ (\mathrm{theo})\ {}^{+0.0008}_{-0.0054}\ (\mathrm{pdf})$

World Average

$\alpha_s(M_Z) = 0.119 \pm 0.004$ (S. Bethke hep-ex/9812026)

Figure 18: Comparison of the preliminary values of $\alpha_s(M_Z)$ determined from the analysis of the inclusive jet cross section [38] with the present results determined from the measurement of the dijet event rate for the the factorizable k_T and the modified Durham algorithm. Also shown is the current world average value for $\alpha_s(M_Z)$ [40].